JGR Oceans

RESEARCH ARTICLE
10.1029/2019JC015267

The Surface Pathways of the South Atlantic: Revisiting the Cold and Warm Water Routes Using Observational Data

K. L. Drouin[1] and M. S. Lozier[1]

[1]Earth and Ocean Sciences Department, Nicholas School of the Environment, Duke University, Durham, NC, USA

Key Points:

- Two main observational data sets are used to map the pathways of the upper limb overturning circulation in the South Atlantic
- The Benguela Current sources its waters from the Pacific Ocean, the Agulhas Current, and the subtropical basin interior
- Pacific Ocean and Indian Ocean waters interact throughout the South Atlantic basin, with the latter contributing less than suggested by previous publications

Correspondence to:
K. L. Drouin,
kimberley.drouin@duke.edu

Citation:
Drouin, K. L., & Lozier, M. S. (2019). The surface pathways of the South Atlantic: Revisiting the cold and warm water routes using observational data. *Journal of Geophysical Research: Oceans*, *124*,7082 –7103.https://doi.org/10.1029/2019JC015267

Received 6 MAY 2019
Accepted 5 SEP 2019
Accepted article online 11 SEP 2019
Published online 23 OCT 2019

Abstract The relative contributions of the Atlantic Meridional Overturning Circulation upper limb source waters in the South Atlantic (SA) remain largely unresolved. We contribute to a resolution by using observational data to explore water mass pathways feeding into the Benguela Current, considered a major component of the Atlantic Meridional Overturning Circulation upper limb in the SA. We focus on the pathways from the Pacific Ocean via the Drake Passage (traditionally termed the "cold" water route) and the Indian Ocean via Agulhas Leakage (traditionally termed the "warm" water route). We employ two main observational data sets: (1) surface drifter trajectories from the National Oceanic and Atmospheric Administration's Global Drifter Program and (2) the Ocean Surface Current Analysis Real-time product. Based on our Lagrangian analysis, the majority of particles originating in the Drake Passage remain in the Antarctic Circumpolar Current, with a small portion reaching the northern limb of the SA subtropical gyre, and a few infiltrating the Agulhas Current region. The majority of particles released in the Agulhas Current follow the Agulhas Return Current and recirculate in its vicinity. Only a small portion leaks into the SA. Observed pathways reveal strong interactions between the two source waters in the Brazil-Malvinas Confluence, the SA subtropical gyre, the Benguela Current, and the Agulhas Current region. Results from backward trajectories suggest a sizable contribution of waters from the Drake Passage to the Benguela Current but show disagreement between the two datasets in the magnitude of this contribution.

Plain Language Summary The Atlantic Meridional Overturning Circulation is an important component of the climate system. The relative proportion of the source waters that comprise the upper limb of this circulation in the South Atlantic is still debated. Here we investigate the surface pathways of source waters from the Pacific and Indian Oceans using two main observational data sets. Specifically, we use ocean drifters and a satellite and in situ data derived ocean surface current product. We find that source waters from the Pacific and Indian Oceans share many pathways throughout the South Atlantic basin, especially in the gyre and boundary regions. The source waters of the Benguela Current, which merges waters of the upper limb, stem from the South Atlantic interior, the Pacific Ocean, and the Indian Ocean. The contribution of the Pacific Ocean is larger than recently assumed, while the contribution from the Indian Ocean is on the lower end of previous estimates from the literature.

1. Introduction

The Atlantic Meridional Overturning Circulation (AMOC) consists of a northward flowing warm and salty upper limb, which compensates a southward flowing cold and fresh lower limb. While this overall depiction of the northward heat flux throughout the Atlantic basin is well understood (Garzoli & Matano, 2011) relative contribution of the source waters for the upper limb in the South Atlantic is still debated. Specifically, there is disagreement as to whether the upper limb of the AMOC is primarily fed by cold, fresh waters from the Pacific Ocean, which enter the SA basin through the Malvinas Current (MC) via the Drake Passage (DP), or by warm, salty waters from the Indian Ocean, which enter the South Atlantic (SA) via Agulhas leakage in the form of mesoscale eddies and filaments. The former is traditionally referred to as the "cold water route" following (Rintoul, 1991), while the latter is termed the "warm water route" following (Gordon, 1986). It has also been suggested that a minor contribution to the source waters of the upper limb stems from local water masses formed within the SA (Stramma & England, 1999).

Interest in these competing sources stems from an expectation that the prevalence of one over the other affects the variability and stability of the AMOC because of their influence on deep water formation in the

North Atlantic (Garzoli & Matano, 2011). For example, Beal et al. (2011) suggest that salinity input via Agulhas leakage acts as a stabilizing mechanism for the AMOC by offsetting freshwater forcing in the North Atlantic. However, modeling results from Weijer and van Sebille (2014) indicate that such salinity input would be too weak to change the stratification of the North Atlantic. Since several studies suggest that Agulhas leakage has increased over the past few decades (Biastoch et al., 2009; Durgadoo et al., 2013) and another predicts a continued increase under current climatic conditions the relative contribution of the warm water route continues to be of interest.

In the years since the seminal studies of Gordon (1986) and Rintoul (1991), numerous studies have tried to quantify the relative importance of these two pathways, with no consensus to date (Garzoli & Matano, 2011). Gordon et al. (1992) attempted to reconcile the two viewpoints by suggesting an indirect contribution from the Pacific waters. The authors suggested that waters entering the SA via the DP follow the Antarctic Circumpolar Current (ACC) eastward, are subsequently entrained in the Indian Ocean subtropical gyre and then eventually merged with the Agulhas Current (AC) to reenter the SA basin via Agulhas leakage. This route forms part of the super-gyre that connects the Indian, Pacific, and Atlantic Ocean basins (De Ruijter, 1982; Speich et al., 2007).

Both the warm water route (Donners & Drijfhout, 2004; Lee et al., 2019; Speich et al., 2001; Speich et al., 2007; Weijer et al., 2002) and the cold water route (Macdonald, 1998; Sloyan & Rintoul, 2001; You, 2002) have found heavy favor in past studies. Two recent studies, however, suggest a more comparable role for the pathways, while still attributing a larger contribution to the warm route (Rodrigues et al., 2010; Rühs et al., 2019) The divergent estimates of the cold and warm water route contributions can be partially explained by the use of different data sets and methods, as well as the use of coarse-resolution models (Donners & Drijfhout, 2004; Rühs et al., 2019)

The majority of these past studies have addressed the contributions of the cold and warm water routes from a modeling perspective, either in the Eulerian or Lagrangian framework. The purpose of this study is to reinvestigate the source waters of the AMOC upper limb in the SA using observational data. The observational data sets available for this study—surface drifters and satellite derived ocean surface current fields—yield information on surface velocities only. To alleviate this constraint, we qualitatively compare the surface drifter trajectories to subsurface floats. However, since these floats are primarily isobaric, they too are unable to capture the full three-dimensional pathways. We admit the constraint placed on this study by this limitation, but in the absence of three-dimensional velocities from the observational record, surface pathways can provide valuable, albeit imperfect, information about the circulation (Mariano et al., 2002; van Sebille et al., 2011). Our purpose then is not to produce a comprehensive assessment of the upper limb pathways but rather to understand what we can learn about surface pathways in the SA, as they pertain to the AMOC upper limb, from the observational database alone. A follow-on study, using numerical modeling output, will examine the full three dimensionality of the pathways. As such, this present study will also provide important validation for the modeled pathways.

To meet our goal of using available observations to assess surface pathways in the SA, we produce three sets of trajectories: those directly available from surface drifters, those computed from a Markov chain using the surface drifter record, and those computed from surface velocity fields. Additionally, we compare the surface drifter trajectories to subsurface float trajectories. An inspection of the similarities and differences among these sets allows for a more robust evaluation of the surface pathways. Finally, we note that our goal is a description of the mean, rather than temporally varying pathways. The remainder of this paper is organized as follows: Section 3 provides an overview of the observational datasets and methods; section 4 presents and discusses the results; and section 4 summarizes the findings.

2. Data and Methods

We define our study region between 70°S–10°S and 70°W–50°E and refer to it as the SA domain (Figure 1). For the analysis of the Markov chain and the trajectories computed from surface velocity fields, we further define four geographical subdomains: the northern SA, the southern SA, the Agulhas Region (AR), and the DP (Figure 1).

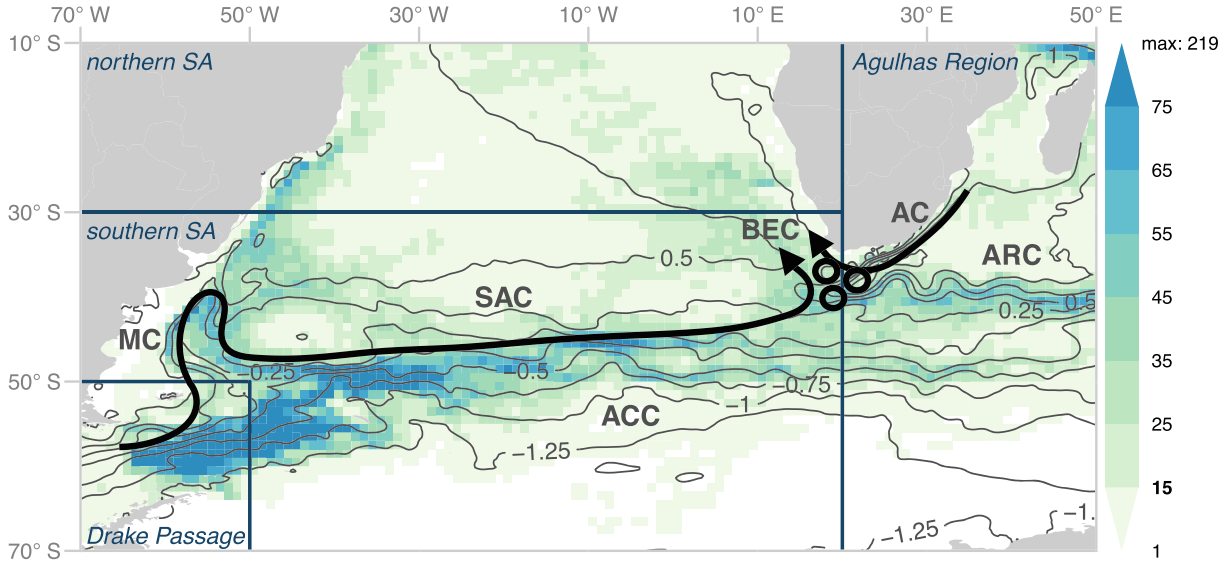

Figure 1. Map of the SA domain with the names of relevant ocean currents. Specific study regions are demarcated by dark blue lines. The northern SA is defined between 70°W and 20°E and 30°S and 10°S; the southern SA is defined between 70°W and 20°E and 70°S and 30°S with the exception of the region defined between 70°W and 50°W and 70°S and 50°S, which is defined as the Drake Passage; the Agulhas Region is defined between 20°E and 50°E and 70°S and 10°S. Black contours (0.2-m intervals) are the absolute dynamic topography in meters from AVISO. The background shading indicates the number of GDP drifters per one-by-1° grid box. Grid boxes containing less than the median number of drifters (15) are colored in the same color. The schematic pathways and eddies highlight the traditional cold route from the Pacific Ocean (Gordon, 1986) and warm route from the Indian Ocean (Rintoul, 1991). The abbreviations denote the following ocean currents: AC = Agulhas Current; ACC = Antarctic Circumpolar Current; ARC = Agulhas Return Current; BEC = Benguela Current; MC = Malvinas Current; SAC = South Atlantic Current.

Our focus lies on the identification of pathways from the DP (waters entering the SA across 70°W) and the Agulhas Current (AC; water flowing across 32°S between 30°E and 35°E), as well as pathways to the Benguela Current (BEC; waters crossing 30°S between 0° and 15°E). Since this work primarily addresses the geographical origins and pathways of the surface waters of the SA, the cold and "warm" water routes are henceforth referred to as "Drake Passage" and "Agulhas" waters, respectively.

Previous studies involving the upper limb of the AMOC have chosen the North Brazil Current as a region of interest as it acts as a bottleneck for the waters of the upper limb (Rühs et al., 2013; Rühs et al., 2019). However, past studies have indicated that the connection to the North Brazil Current is at least partially subsurface (Johns et al., 1998; Schott et al., 1998; Schott et al., 2005; Stramma, 1991). A relatively recent study, for example, showed that only 1% of surface trajectories released in the Agulhas Current would reach the North Atlantic over 100 years, a value that increases to 2% when the three-dimensional nature of the pathway is taken into account (van Sebille et al., 2011). To minimize the impact of the surface constraint on our study, instead of choosing the North Brazil Current as the end point for trajectories released at the source locations, we use the upstream BEC. This current is also sourced by the same Pacific and Indian Ocean waters (Garzoli & Gordon, 1996; Garzoli & Matano, 2011) yet is located much closer to the source locations.

We use two observational data sets to produce surface pathways: (1) satellite-tracked surface drifters from the National Oceanic and Atmospheric Administration's Global Drifter Program (GDP; publically available for download at: https://www.aoml.noaa.gov/phod/gdp/index.php) and (2) the Ocean Surface Current Analysis Real-time (OSCAR) generated by Earth Space Research (publically available for download at: https://podaac.jpl.nasa.gov/dataset/OSCAR_L4_OC_third-deg). We use a third observational data set, subsurface floats from the World Ocean Circulation Experiment Subsurface Float Data Assembly Center (WFDAC) at Woods Hole (publically available for download at: https://www.aoml.noaa.gov/phod/float_traj/data2.php), to compare our surface trajectories to subsurface trajectories. These datasets are discussed further in the following sections, as is our use of a Markov chain to compute pathways. For a discussion and maps of the OSCAR and surface drifter velocity fields we refer the reader to Johnson et al. (2007), Dohan and Maximenko (2010), and Laurindo et al. (2017).

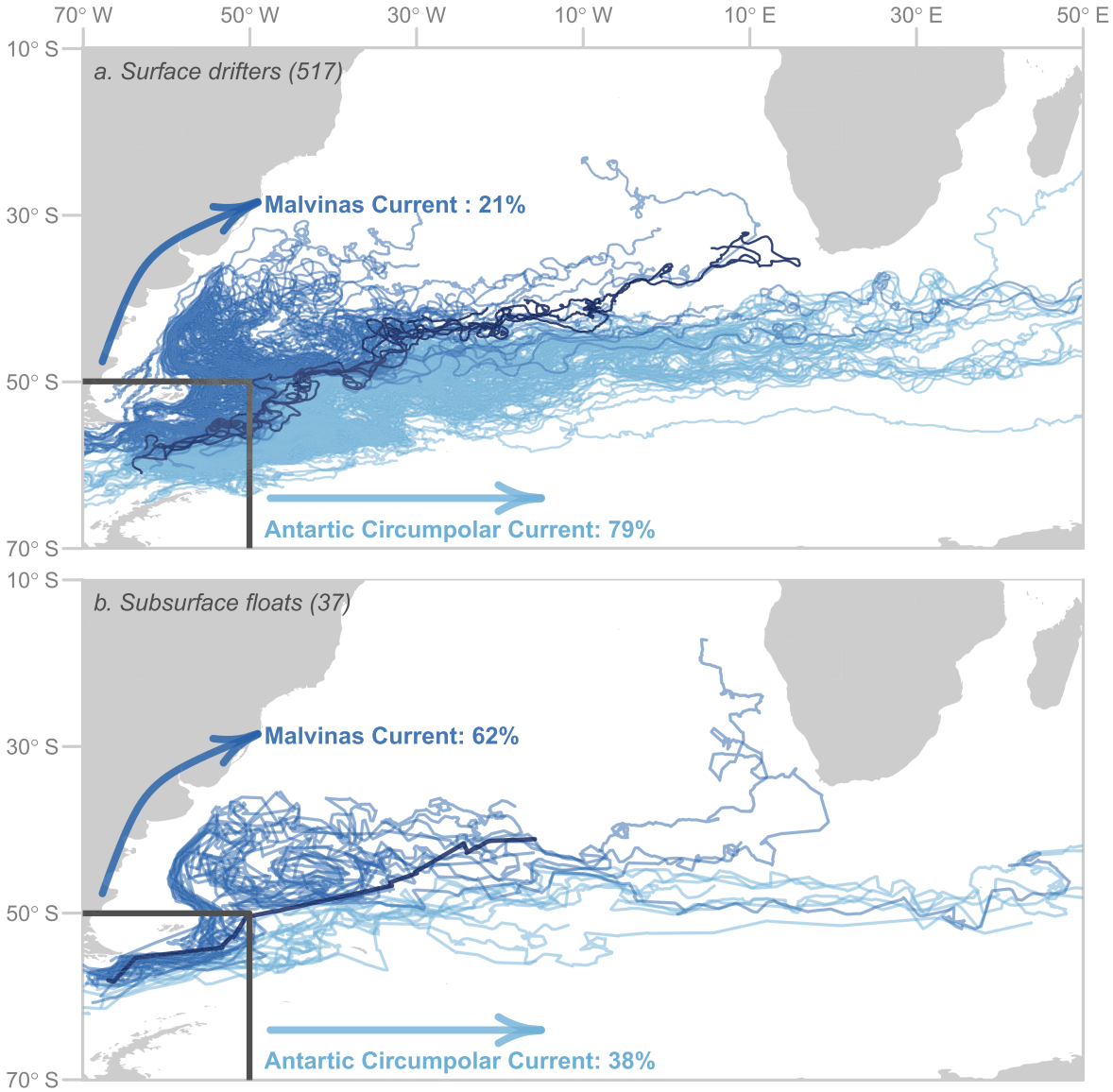

Figure 2. Surface drifter and subsurface float trajectories from the Drake Passage. (a) Trajectories of 517 drifters passing through the grey box (70°S–50°S, 70°W–50°W). The drifters are colored by their preferred pathways: Drifters entering the SA in the MC are colored in blue; drifters remaining in the ACC are colored in light blue. Drifters that enter the SA in the ACC but, subsequently, become entrained in the MC are counted as MC drifters. Drifters that escape the ACC and travel on a more northerly route are colored in dark blue. (b) Similar to (a) but for the trajectories of 37 floats passing through the DP. The average depth of the floats is 783 ± 159 m with a range of 50–1,554 m. Note that there is an updated version of this float data set available, however, the version we employ (version 1.0) has identical data to the newer version (version 2.0) in the SA. The 37 floats include 36 ALACE floats and 1 PALACE float.

2.1. Surface Drifters and Subsurface Floats

The GDP surface drifter data consists of 15-m drogued and undrogued drifters, whose longitudinal and latitudinal positions are reported every 6 hr. Here the full GDP data set is subsampled to include surface drifters, henceforth referred to as "drifters," passing through our SA domain (Figure 1) between November 1989 and June 2018. Since undrogued drifters do not accurately capture the motion of near-surface currents (Lumpkin & Pazos, 2007; Niiler & Paduan, 1995; Pazan & Niiler, 2001), their trajectories are excluded from this analysis. However, the trajectories of drifters that have lost their drogue are included up to the point of drogue loss. Given these constraints, the SA GDP data set is comprised of 3,425 trajectories. Note that while this full SA GDP data set is used for the construction of the Markov chain, the qualitative analysis of the drifter trajectories only includes drifters that are located in the vicinity of the DP, the AC, and the BEC (Figures 2–5) and have a minimum lifetime of thirty days.

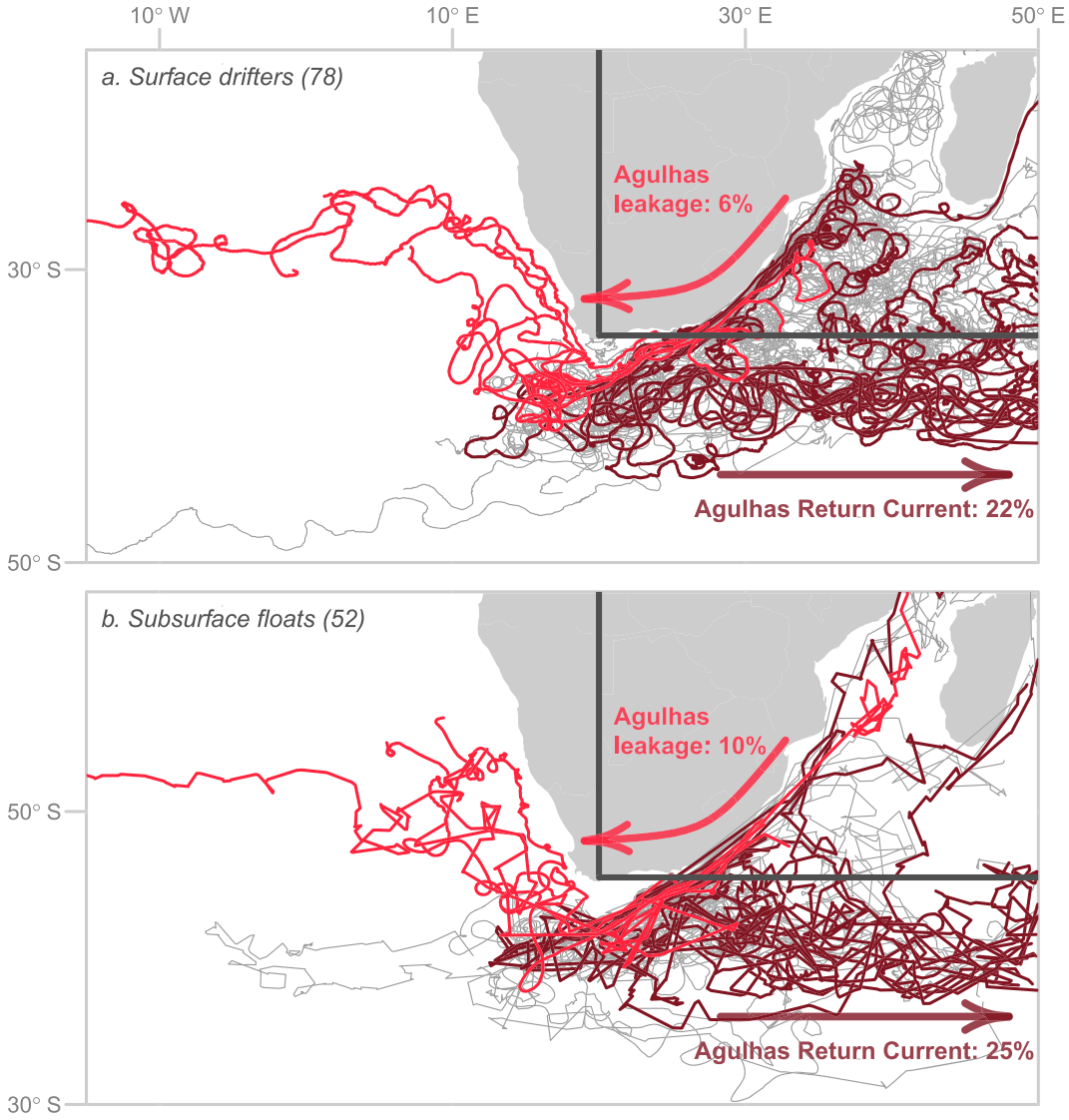

Figure 3. Surface drifter and subsurface float trajectories from the Agulhas. (a) Trajectories of 78 drifters passing through the grey box (34.5°S–15°S, 20°E–50°E). The drifters are colored by their preferred pathways: Drifters leaking into the SA are colored in red; drifters that follow the ARC and subsequently exit the domain via the ARC are colored in dark red. Drifters that do not leak or exit through the ARC are colored in grey. (b) Similar to (a) but for the trajectories of 52 floats. The average depth of the floats is 678 ± 332 m with a range of 4–1,294 m. The 52 floats include 17 ALACE floats, 16 PALACE floats, and 19 RAFOS floats.

Our analysis of the drifters is constrained by their limited temporal and spatial coverage. The average lifetime of the drifters used in this study is 0.5 ± 0.5 years. Additionally, their spatial coverage is nonuniform (Figure 1), as it is subject to sampling bias from cruise routes and targeted sampling strategies. The mean number of drifters per 1° grid box is 22 ± 23. As explained in the next subsections, we remove the lifetime constraint of the observed drifters with the use of a Markov chain (McAdam & van Sebille, 2018; Miron et al., 2017; Miron et al., 2019; van Sebille et al., 2012). We also address the bias from the non-uniform drifter distribution by using the satellite-derived OSCAR fields to compute Lagrangian pathways, also described below.

Most significantly, the drifters are drogued to a depth of 15 m and constraint to the surface. Hence, as mentioned in the introduction, they do not capture the three dimensionality expected from water pathways. To partially account for the lack of three dimensionality, we qualitatively compare the

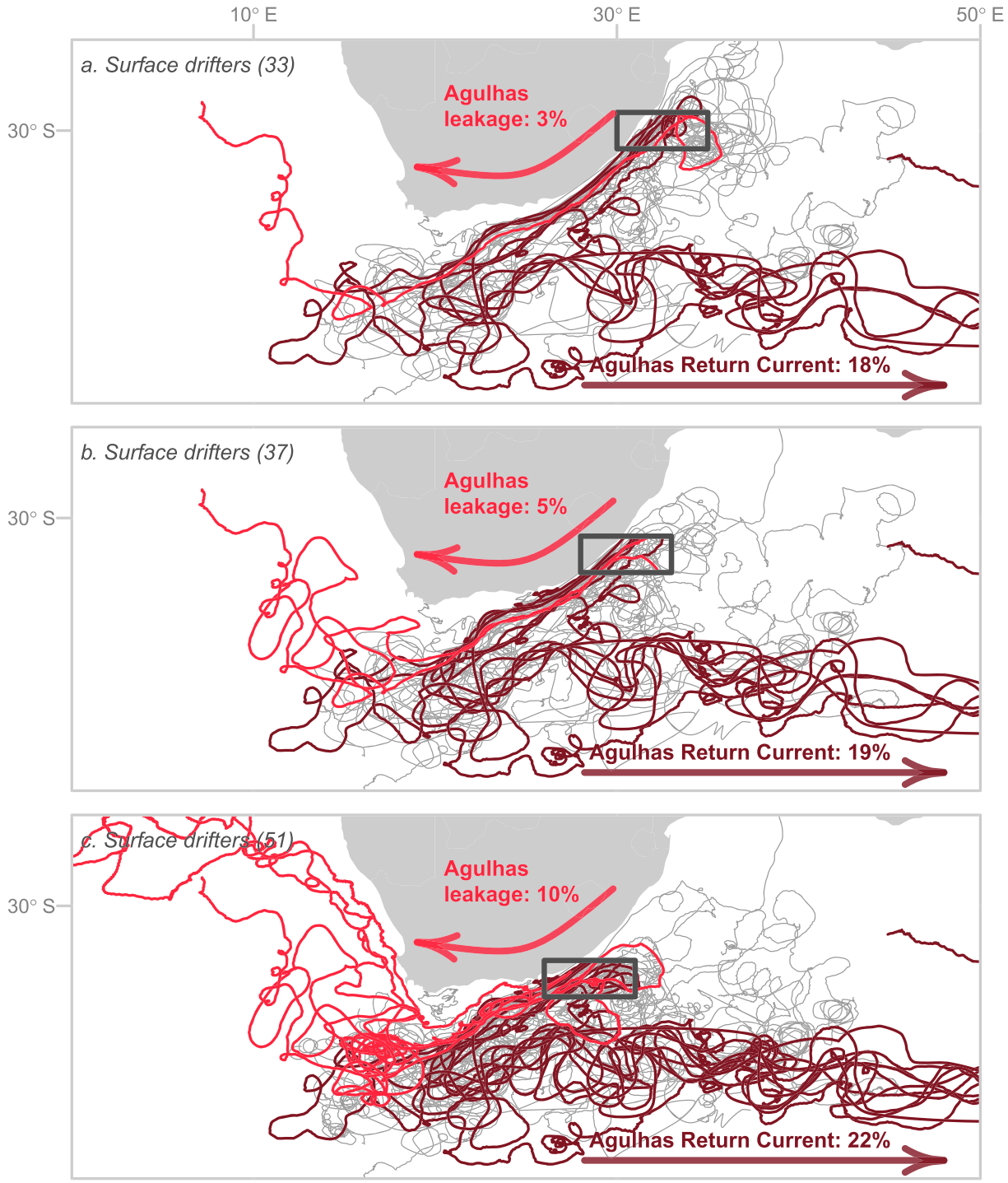

Figure 4. Sensitivity of Agulhas leakage estimates. The colors are as defined in Figure 3 caption. The (a) 33 drifter trajectories passing through the AC at 30°S (grey box). The (b) 37 drifter trajectories passing through the AC at 32°S (grey box). The (c) 51 drifter trajectories passing through the AC at 34°S (grey box).

drifters to subsurface floats available through WFDAC. We highlight again that these subsurface floats, henceforth referred to as "floats," are primarily isobaric and, hence, still do not reflect three-dimensional pathways. As mentioned in the introduction, an investigation of three-dimensional and subsurface pathways awaits further study.

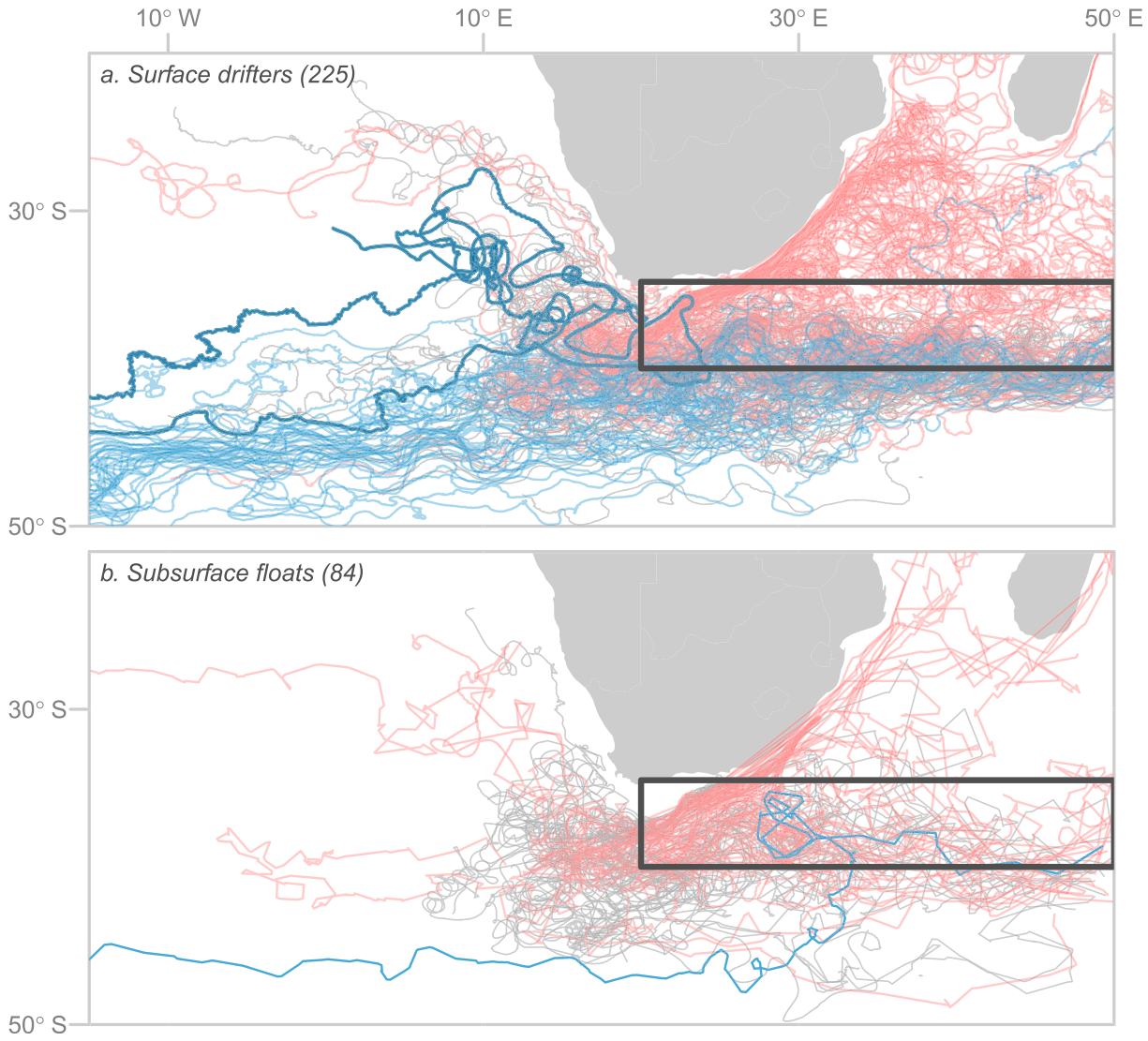

Figure 5. Surface drifter and subsurface float trajectories in the ARC. (a) Trajectories of 225 drifters passing through the grey box (37°S–34.5°S, 20°E–50°E) at any point during their lifetime. Blue drifters originate west of 10°W and south of 40°S. Red drifters originate within the Agulhas domain defined in Figure 3 (34.5°S–15°S, 20°E–50°E). Grey drifters originate elsewhere in the domain. (b) Same as (a) but for the trajectories of 84 floats passing through the vicinity of the ARC. The 84 floats include 28 ALACE floats, 17 PALACE floats, and 39 RAFOS floats.

2.2. Markov Chain From Surface Drifter Trajectories

In general, a Markov chain describes the transition from a present state to a future (or past) state, based on probability distributions. In this context, it serves as a tool to explore oceanic surface pathways and connections implicit in the drifter record on a longer time scale (McAdam & van Sebille, 2018; van Sebille et al., 2012). A detailed description of the use of Markov chains and their limitations in oceanographic applications can be found in (McAdam & van Sebille, 2018). Though we acknowledged the limits imposed by drifter coverage above, we note here that the validity of the Markov chain is not influenced by the non-uniform sampling of the drifters (see Miron et al., 2019 for details).

To construct the Markov chain from the GDP drifter data, we divide the domain into a discrete grid with a horizontal resolution of dx and dy. Next, we split the drifter trajectories into subtrajectories of length dt and consider all positions at time $t = t_o$ in a specific grid cell and find the position of those drifters at time $t = t_o + dt$. We then determine the probability of moving from that grid to another grid over the time step dt. We repeat this step for all grid cells and summarize the probabilities in a transition matrix. After

determining all probabilities for all grids, we initialize particles in a specific grid and compute their probabilistic trajectories over 5 years.

The steps outlined above largely follow the method outlined in McAdam and van Sebille (2018) with two exceptions: First, we normalize the drifter trajectories by the total number of drifter trajectories in a grid cell at time $t = t_o$, rather than by the number of drifter trajectories that leave a given grid cell over the time step dt. This modification accounts for drifters that remain in a given grid cell over the assigned time step dt. Second, we construct the transition matrix using only the trajectories of drogued drifters, due to the limitations of undrogued drifters described above.

Here we also construct a "backward" Markov chain to trace surface waters back to their sources. In this case, the probability distribution for each grid cell is calculated based on the drifter position at time $t = t_o$ and $t = t_o - dt$.

2.2.1. Markov Chain Parameters

Following McAdam and van Sebille (2018), the spatial grid for the Markov chain is set to $dx = dy = 1°$, which yields a total of 4,887 grid cells in our SA domain. We take advantage of the full SA drifter data set and split the 2,983 drifter trajectories into roughly 2.1 million subtrajectories. This yields an average of 860 ± 686 observations per grid cell, with 237 grid cells (5%) containing less than 50 observations. Note that approximately 1% of the grid cells are absorbing, that is, once a drifter enters an absorbing grid cell it remains there indefinitely, since there is a zero probability of leaving an absorbing grid cell (Miron et al., 2017; van der Mheen et al., 2019). Accordingly, we exclude the absorbing grid cell from our analysis (van der Mheen et al., 2019).

We define dt as the advective time scale for surface particles. A simple scaling analysis, with a nominal length scale of 40–100 km and velocities of 0.1–1 ms^{-1}, yields a range for dt of 0.5–10 days. We justify our choice of the midrange value ($dt = 5$ days) as follows. First, we conducted sensitivity simulations using $dt = 1$, 5, 10, and 100 day(s) and used two metrics to compare the actual drifter positions to the positions predicted by the Markov chain particles. To ensure the best comparison, we subsampled the drifter trajectories to the time step of each Markov chain. Specifically, we calculated (1) artificial dispersion, defined as the number of grid cells occupied by Markov particles that are not occupied by the original drifters, normalized by the total number of grid cells occupied by the Markov particles and (2) undercapture, defined as the number of grid cells occupied by the original drifters that are not occupied by the Markov chain particles, normalized by the total number of grid cells occupied by the original drifters. Ideally, both quantities should be minimized. A comparison of these metrics for all tested dt values reveals that after 300 days, $dt = 5$ days gives a relatively low artificial dispersion (~14%) and small undercapture (~10%). For $dt = 1$ day and $dt = 100$ days, the artificial dispersion is ~15% and ~40% and the under-capture is ~12% and 35%, respectively. Additionally, a time scale of 5 days exceeds the Lagrangian decorrelation time scale of the surface ocean of two to three days (LaCasce, 2008) meaning that the velocity field is memoryless after five days. This loss of memory is a requirement for the Markov chain (Miron et al., 2017). Finally, this advective timescale also matches the temporal resolution of the OSCAR fields. For more information on artificial dispersion in Markov chains, the reader is also referred to McAdam and van Sebille (2018).

Ideally, one could construct a three-dimensional Markov chain from the subsurface floats. However, their limited number (480), which results in an average coverage of 4 ± 4 floats per grid cell (compared to an average of 22 ± 23 surface drifters per grid cell), coupled with their scattered distribution throughout the SA and irregular reporting time, precludes this possibility.

2.3. Lagrangian Particle Simulations in OSCAR

The OSCAR fields are two-dimensional velocity fields representative of the upper 30 m of the ocean and are computed from quasi-linear and steady flow momentum equations using in situ measurements and satellite altimetry data as input (Bonjean & Lagerloef, 2002). These velocities are available globally at a spatial resolution of one-third degree and a temporal resolution of 5 days. For this study, we use the 2000–2017 OSCAR fields covering our SA domain. Prior years are excluded from this study as they do not have enough data coverage close to the South African coast.

To optimize the comparison between the drifter trajectories, the Markov chain, and the Lagrangian particle simulations using OSCAR, we release particles daily over a period of 10 years. The particles are advected

forward in time from the DP and AC, as well as backward in time from the BEC using a fourth-order Runge-Kutta integration scheme with a time step of 1 hr. Over the 10-year period, trajectories are integrated for 5 years, with positions recorded every 5 days. The OSCAR fields are interpolated to each particle position at each time step bicubically in space and linearly in time. To minimize the number of particles advected onto land, particles close to land (i.e., 1°) are advected using the Forward Euler method instead of the Runge-Kutta scheme. Additionally, in these cases the velocities are not interpolated and only the component parallel to the coast of the closest available velocity is used for the integration.

For our analysis of the OSCAR pathways, we only include particles that last the whole integration period, leave the domain prior to 5 years (DP and AC), or reach the source regions prior to 5 years (BEC). For the DP and BEC simulations, approximately 90% of launched particles match these criteria. For the AC simulations this value is slightly lower, at around 75%. The majority of particles are lost close to the shore, due to a lack of data coverage and the needed interpolation and integration scheme. Note that approximately 8% are lost from each launch site, meaning that no one launch site experiences more or less loss than any other.

2.4. Data Analysis

The GDP drifter trajectories are qualitatively analyzed in terms of their preferential pathways and quantitatively in terms of their travel time to certain sections of the domain. The WFDAC subsurface float trajectories are used as a qualitative comparison of pathways for the surface drifter trajectories.

We create two different probability maps for the results of the Markov chain (Figures 7–9) and the OSCAR fields (Figures 10–12). For the first map, we count the number of particles that pass through each grid cell over 5 years and normalize this count by the total number of particles released. Note that each particle is only counted once per grid cell. As such, each grid cell can have a maximum value of 100% if all released particles pass through that particular grid cell over the 5-year integration time period. This distribution map highlights preferential pathways, since high particle concentrations denote the routes that most of the particles follow.

For the second map, we count the total number of particle positions in each grid cell over the course of 5 years and normalize this count by the total number of particle positions of all released particles. Thus, the cumulative sum of all grid cells is 100%. While this type of distribution map also shows preferential pathways, it primarily highlights areas of large residence time. Combining these two views allows us to, for example, determine if high particle concentrations result from many particles following a specific path or from strong recirculation in the area (van Sebille et al., 2018).

3. Results and Discussion

In section 4.1, we discuss what can be inferred from the original GDP data set by qualitatively analyzing the trajectories of drifters passing through the DP, the AR, and the BEC and qualitatively compare the trajectories to subsurface floats. In sections 4.2 and 3.3, we take a more quantitative approach and discuss the results of the Markov chain and OSCAR particle advections, respectively, in the same regions.

3.1. Surface drifter and subsurface float trajectories

3.1.1. Drake Passage

A total of 517 drifters enter our SA domain through the DP (Figure 2). One fifth of those divert to the north and enter the MC (21%; blue), while the rest remain in the ACC (79%; light blue). The drifters entering the MC primarily pass through the DP north of 60°S. The entanglement, looping, and eddying motion of the MC drifters highlight the energetic and dynamic nature of the Brazil-Malvinas Confluence (Garzoli, 1993; Jullion et al., 2010; Willson & Rees, 2000). As the drifters move eastward, a few that had followed the MC (blue) subsequently rejoin the ACC, while a few others that had been following the ACC are entrained into the South Atlantic Current (dark blue), highlighting continuous exchange between the two currents (Boebel et al., 1999). Though a previous study had suggested a lack of exchange between the ACC and the South Atlantic Current after 50°W (Speich et al., 2001), our results show continuous exchange up to approximately 35°W, in agreement with previous work by Boebel et al. (1999) and a recent modeling study by Rühs et al. (2019). Some drifter trajectories follow intra-gyre pathways in the SA basin (Figure 2), an observation in agreement with a modeling study by (Schmid, 2014). The author suggests that the South Atlantic Current

may be connected to the southern South Equatorial Current via pathways that cross the interior of the subtropical gyre.

Approximately 20% of drifters travel across 10°W. Of those, the majority are located in the ACC and a smaller fraction (6%) is found in the BEC. Drifters traveling in the ACC (light blue; Figure 2) cross 10°W after 0.9 ± 0.2 years. Drifters travelling via the MC (blue; Figure 2) and subsequently the South Atlantic Current only cross 10°W after 1.7 ± 0.4 years. Given the drifters' relatively short lifetime of 0.7 ± 0.5 years, these transit times are likely underestimated, particularly so for the BEC with its longer transit from the DP. In addition to these two pathways, a number of drifters are entrained into the Agulhas Return Current (ARC), suggesting a possible conflation of the cold water and warm water routes closer to the warm source than previously suggested (Gordon et al., 1992; Speich et al., 2007). As mentioned above, earlier work addressed the interaction between the DP waters and Agulhas waters outside of the SA basin. Their primary focus was on DP water recirculating within the Indian Ocean subtropical gyre or entering the Indian Ocean through Tasman Leakage to form a super-gyre (Gordon et al., 1992; Speich et al., 2001; Speich et al., 2007). Instead, here we suggest a mixing of these two sources just southeast of the African continent. Further evidence for this is discussed in the context of Figure 5.

The subsurface float trajectories (Figure 2b) qualitatively agree with their drifter counterparts (Figure 2a). Again, there are two prominent pathways: One follows the ACC, and the other is along the MC and the South Atlantic Current (Peterson & Stramma, 1991; Schmid, 2014). However, in contrast to the drifters, a larger percentage of floats takes the latter route (62%) than the former route (38%). With the caveats of a relatively small sample size (37 floats) and the fact that most of the floats are located in the northern DP, this difference might indicate that the MC dominates at the subsurface. The floats have a longer average lifetime (2.5 ± 1.7 years) than the drifters (0.7 ± 0.5 years). Given this extended lifetime, a larger fraction of floats (37%; Figure 2b) crosses 10°W, compared to the drifters (21%; Figure 2a). As with the drifters, the travel time to the BEC is longer (5.6 ± 0.1 years) than the travel time to 10°W in the ACC (3.7 ± 1.4 years).

3.1.2. Agulhas

Seventy-eight drifters are found in the Agulhas domain (Figure 3a). These drifters have an average lifetime of 0.8 ± 0.5 years. The majority of these drifters (72%) stay in the Indian Ocean without leaking into the SA or following the ARC (Figure 3a; grey). A total of 22% exit the domain via the ARC, a few of which subsequently reenter the domain (Figure 3a; dark red). The strong looping and entanglement of the drifter trajectories (Figure 3a) highlights the enhanced eddy activity near the AC and ARC (Biastoch & Krauss, 1999). Approximately 6% of drifters (red) leak into the SA, defined here as crossing 32°S west of 20° E (Figure 3a).

The float trajectories (Figure 3b) again show qualitatively similar pathways to the drifter trajectories (Figures 3a and 3b). At depth, fewer floats exhibit the looping motion observed in the drifters, and the large majority (71%) exits the domain via the ARC (Figure 3c). Keeping the relatively low number of float trajectories in mind, the amount of leakage seems to be higher at depth (10%).

We emphasize here that the abovementioned percentages are very sensitive to the sampling criteria used (Figure 4). For instance, by using a stricter definition of Agulhas leakage and only including those drifters that pass directly through the AC at 30°S, we observe only one drifter (3%) leaking into the SA (Figure 4a). Repeating this for the latitudes 32°S and 34°S, we obtain 5% and 9%, respectively (Figures 4b and 4c).

These various leakage estimates (3%–9%) are notably lower than previous estimates using the GDP drifters, which range from 25% to 33% (Richardson, 2007; van Sebille et al., 2009). To test whether this discrepancy can be explained by the use of data from different time periods, we resampled the drogued drifters to match the time periods used in these two previous studies: 1994–2004 for Richardson (2007) and 1995–2008 for van Sebille et al. (2009). We calculate Agulhas leakage of 14% and 11% for the 1994–2004 and 1995–2008 periods, respectively (using the 30°S definition of the AC; Figure 4a). Note that the only drifter that leaks into the SA over the shortened time periods is the drifter shown in Figure 4a.

As highlighted above (Figure 4), differences in drifter sampling influence leakage estimates. Since Richardson (2007) does not explicitly state how he defines AC drifters, a likely explanation for the difference in leakage estimates is the difference in what is or is not considered an AC drifter.

However, we suggest that the discrepancy in these estimates mainly arises because Richardson (2007) and van Sebille et al. (2009) included undrogued drifters in their calculations. We note here that the differentiation between drogued and undrogued drifters in the GDP data set received more attention after the publication of these two papers (Lumpkin et al., 2013). The inclusion of undrogued drifters for our time period at 30°S yields a leakage of 19%, still lower than the previous estimates (25%–33%), yet closer to them.

When following our stricter definition of Agulhas leakage discussed above for the drifters and only using floats flowing directly through the AC at 30°S, we observe three floats leaking into the SA, for a leakage value of 11%. This estimate is also lower than a previous estimate made by (Richardson, 2007), who calculated a leakage of 18% using RAFOS floats and 23% using ALACE floats. Since no additional floats were released in that area since Richardson's study, we attribute this difference to the inclusion of a different number of floats according to different sampling criteria.

3.1.3. Interaction Between the Drake Passage and Agulhas

To further evaluate the interaction between the DP and Agulhas drifters, we next consider the trajectories of 225 drifters located in the vicinity of the ARC (Figure 5a). Strong comingling of DP drifters (blue), Agulhas drifters (red), and drifters originating elsewhere in the domain (grey) is observed (Figure 5a). Thus, these surface drifters illustrate that this interaction not only takes place in the BEC (Rodrigues et al., 2010) but also, as discussed above, just south of the African continent where the AC retroflects into the ARC (Boebel et al., 2003), as well as within the ARC itself. Specifically, as previously mentioned, some DP drifters (highlighted in dark blue; Figure 5) are able to enter the ARC and leak back into the SA without taking a detour through the Indian Ocean subtropical gyre. This observation is similar to a pathway described by Rühs et al. (2019), whereby waters in the ACC take a small detour in the Agulhas basin before leaking back into the South Atlantic. Similar behavior is observed in the floats, though the apparent interaction between floats from the DP and AC is weaker due to the limited number of floats (Figure 5b).

3.1.4. Benguela Current

There are 89 drifter trajectories that reach the BEC (Figure 6b), with the majority originating in the SA (grey; 85%). A small fraction can be traced back to the DP (blue; 11%) and an even smaller fraction to the AC (red; 4%). The large contribution of drifters from the SA is in agreement with (Garzoli & Gordon, 1996), who, however, also find a significant contribution from the AC. The number of drifters that can be traced back to the DP is, again, likely limited by the relatively short lifetime of these drifters (1.1 ± 0.8 years) relative to the travel time from the DP to the BEC. Note that the more northerly blue drifters could have also originated in the Brazil Current. Given the relative proximity of the AC to the BEC, the lifetime is unlikely to play a significant role, sampling bias could, however, be a contributing factor. Overall, drifters originating in the DP spread across a larger longitudinal range than the drifters from the AC, which are more concentrated near the South African coast. Drifters from the DP (blue) cross the SA in the relatively broad South Atlantic Current, with their pathways spanning approximately 10° in latitude (Figure 6a). In contrast, the drifters leaking from the Indian Ocean (red) are located in the narrow AC and closely follow the South African coastline (Figure 6a).

Though limited in number, the floats (Figure 6b) similarly highlight an interaction between floats coming from the DP (blue), the Agulhas (red), and elsewhere in the SA (Boebel et al., 2003; Rodrigues et al., 2010). Compared to the drifters, floats from the Agulhas (red) are located further away from the South African shore. Both the Agulhas and DP floats (Figure 6b) follow similar pathways to their drifter equivalents (Figure 6a).

The drifter trajectories examined above have revealed interesting and confirmed known features of the pathways in the SA (Peterson & Stramma, 1991; Schmid, 2014; Stramma & England, 1999). Drifters coming from the DP mainly remain in the ACC, yet some divert northwestward to merge with the MC and subsequently cross the SA basin in the South Atlantic Current. Drifters in the AC largely recirculate in its vicinity or retroflect in the ARC. Only a small number of drifters leak into the SA from the Indian Ocean. We highlight the potential areas for interaction between these two source waters that are apparent from the drifter record: the BEC, the area just south of the African continent and the ARC. Given the limited lifetime of the drifters and their surface constraint, we are limited in the conclusions that can be drawn from this data set alone, yet, are encouraged that the subsurface floats show many qualitative similarities. Not only does the similarity

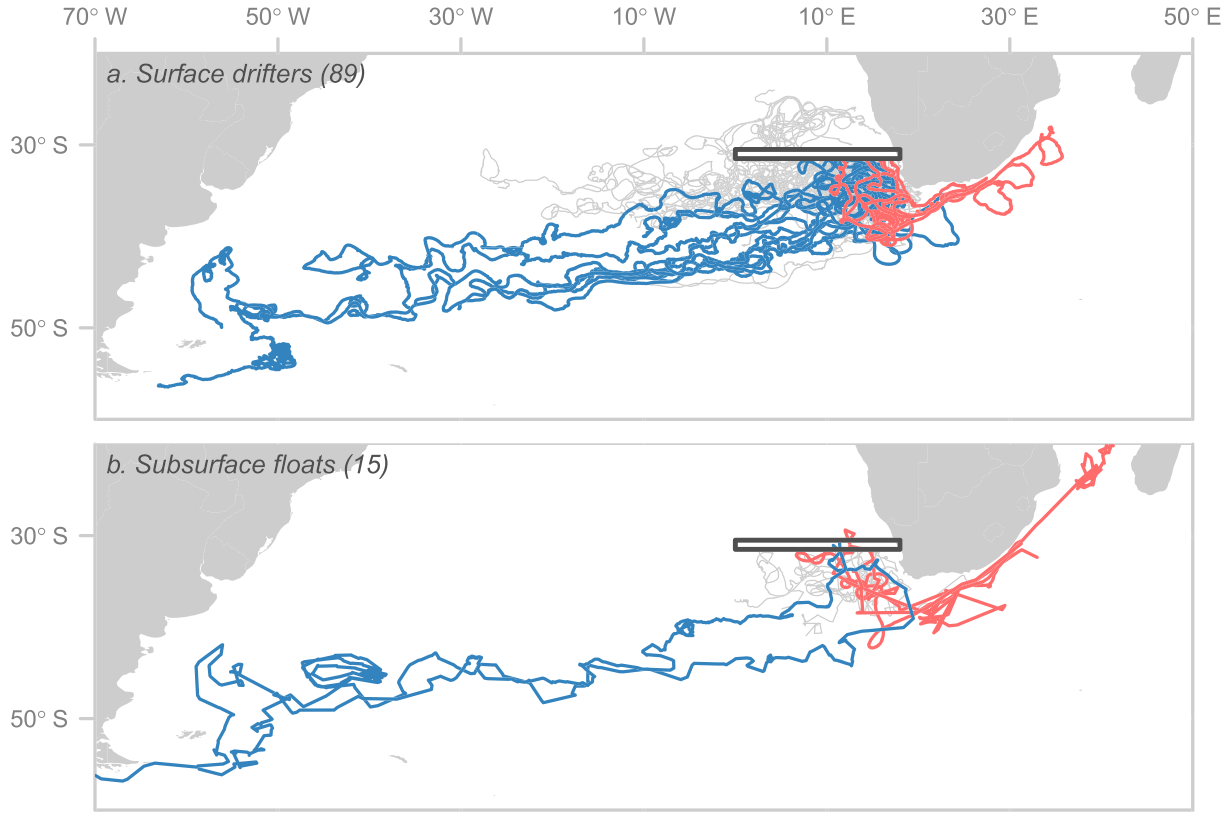

Figure 6. Surface drifters and subsurface floats reaching the Benguela Current. (a) Trajectories of 89 drifters reaching the BEC (grey box). These drifters have an average lifetime of 1.1 ± 0.8 years and are colored by their origin, as defined in Figure 5. (b) Same as (a) but for the trajectories of 15 floats reaching the BEC. The average depth of the floats is 766 ± 232 m with a range of 32–1,039 m. The 15 floats include six ALACE floats, one PALACE float, and eight RAFOS floats.

between these two data sets highlight the well-documented barotropic nature of SA south of 30°S (Killworth & Hughes, 2002; Schmid, 2014; Stramma & England, 1999), it also justifies our use surface drifters to examine pathways in our study region. Next, we turn to our discussion of the Markov chain.

3.2. Markov Chain

For details on the method used to produce the distribution maps of the Markov chain and OSCAR fields, please refer to section 3.4.

3.2.1. Drake Passage

Five years after the launch of particles within the DP, a vast area of the southern SA is occupied by those particles (Figures 7a and 7b). Particles that pass through the DP south of 60°S tend to stay in the ACC and subsequently leave the study domain via the ARC or ACC (Figure 7a). The ACC, MC, and South Atlantic Current are revealed as preferential pathways by the high particle concentrations in Figure 7a. Higher particle concentrations are also observed in the Brazil-Malvinas Confluence, where particles are trapped in its well-documented mesoscale eddy field (Berti et al., 2011; Mason et al., 2017; Olson et al., 1988). The eastern portion of the subtropical gyre is also densely occupied (Figures 7a and 7b), consistent with its relatively sluggish currents. We note that these higher particle concentrations are also likely a result of the two dimensionality of the Markov chain. Specifically, downwelling would presumably reduce the concentration of particles at the surface in areas of horizontal convergence such as this subtropical gyre.

After 5 years, approximately 16% of particles launched in the DP are located in the southern SA (Figure 7a). These particles have either never left the region, returned to the southern SA by completing a circulation in the subtropical gyre, or crossed into the AR and subsequently leaked back into the SA (Figures 7a and 7b). A slightly larger number of particles (17%) can be found in the northern limb of the subtropical gyre

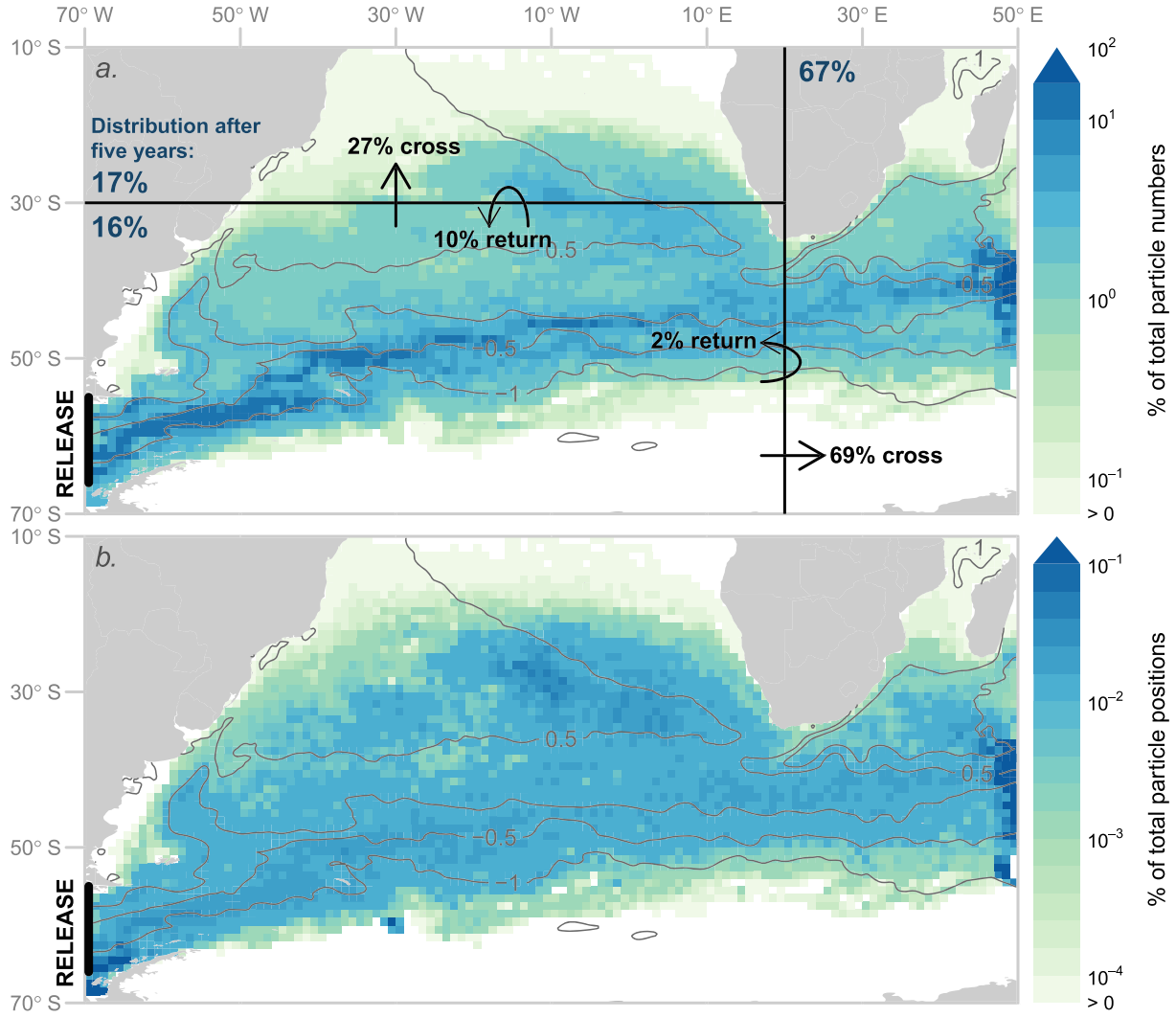

Figure 7. Distribution of Markov chain particles, initialized within the DP along the black line (65°S–57°S; 70°W–69°W), after 5 years. The individual subdomains are demarcated by black lines as defined in Figure 1. (a) Markov chain particle distribution normalized by the total number of released particles. The blue percentages show a snapshot of the particle distribution after 5 years and, thus, sum to 100%. If the particle leaves the domain prior to 5 years, we use its last position in the domain. The straight black arrows indicate the percentage of particles that cross into a given region over 5 years (i.e., they do not sum up to 100% as a particle may cross more than one region over the 5-year period). The curved black arrows indicate the percentage of particles that recirculate between two adjacent regions, that is, they indicate difference between the two previous percentages. Note that the black arrows do not show the exact crossing location of particles. The gray contours show the climatological dynamic topography (m) as derived from AVISO with contour intervals of 0.25 m. (b) Markov chain particle distribution normalized by the total number of particle positions over the course of 5 years.

(Figure 7a). These particles flow northward in the BEC or follow internal pathways that directly connect the South Atlantic Current to the northern limb of the gyre, consistent with (Schmid, 2014).

After 5 years, the largest fraction of particles (67%) can be found east of 20°E in the AR (Figure 7a). While the majority of these particles leave the domain in the ARC (Figure 7a), we observe a smaller number of particles in the vicinity of the AC. Strong recirculations and mesoscale interactions in that region result in the high concentrations shown in Figure 7b.

3.2.2. Agulhas

Qualitatively, the particles launched in the AC largely occupy the same spatial domain (Figures 8a and 8b) as the particles initiated in the DP (Figures 7a and 7b), a similarity especially apparent in the northern limb of the subtropical gyre. Most particles follow the AC (Figure 8a) or recirculate in its vicinity (Figure 8b) and subsequently retroflect to form part of the ARC. Specifically, after 5 years, 80% of particles remain in or return to the Indian Ocean (Figure 8a).

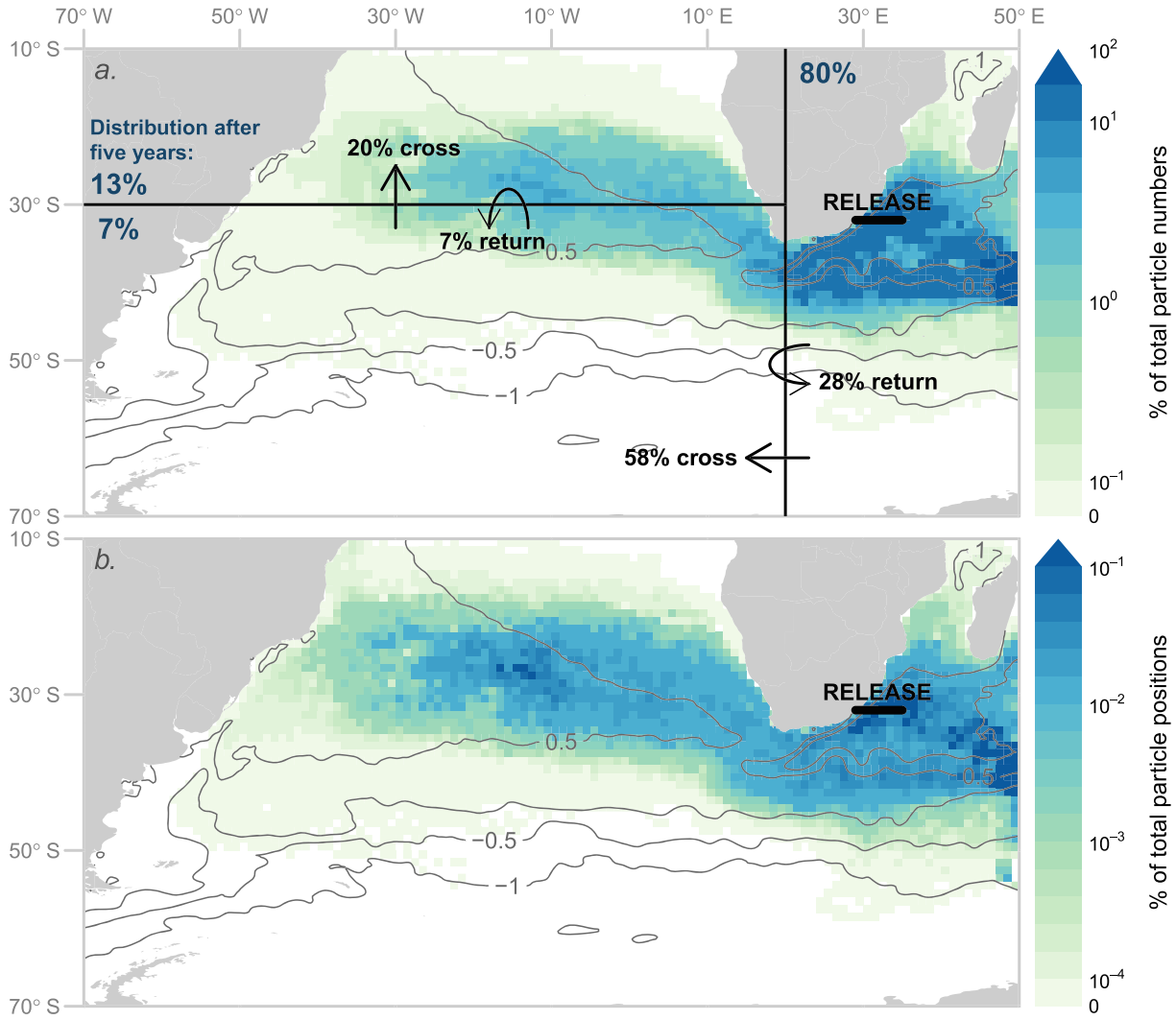

Figure 8. Same as Figure 7 but for Markov chain particles initialized in the AC along the black line (32°S–31°S; 30°–35°E). (a) Markov chain particle distribution normalized by the total number of released particles. (b) Markov chain particle distribution normalized by the total number of particle positions over the course of 5 years. Refer to the Figure 7 caption for additional details.

Approximately 20% of particles leak into the SA (Figure 8a), which is higher than the leakage estimated directly from the drifter record (3%–10%; Figure 4), yet at the low range of the 25%–44% leakage cited in the literature (Durgadoo et al., 2013; McAdam & van Sebille, 2018; Richardson, 2007; van Sebille et al., 2009). In contrast to the particles reaching the BEC from the DP (Figures 7a and 7b), the leaked particles from the AC tightly hug the South African coast and are more concentrated in the eastern part of the BEC (Figures 8a and 8b).

Particles with an AC origin that have leaked into the SA are primarily found in the subtropical gyre around 25°S and 20°W to 10°W (Figure 8b). After 5 years, the 20% of leaked particles are distributed as follows: 13% are located in the northern limb of the subtropical gyre, while a smaller fraction has either remained in or circulated back to the southern SA (7%). Some of the latter particles have invaded the western limb of the subtropical gyre and reached the vicinity of the MC (Figure 8a, b), highlighting a further area of interaction between DP and Agulhas waters.

3.2.3. Benguela Current

Particles initialized in the BEC and traced backward in time fill the entire SA basin after 5 years, indicating that waters originating in the SA may also provide a source for the BEC (Figures 9a and 9b). However, the majority of particles in the BEC can be traced back to the DP (67%) after a period of 5 years (Figure 9a).

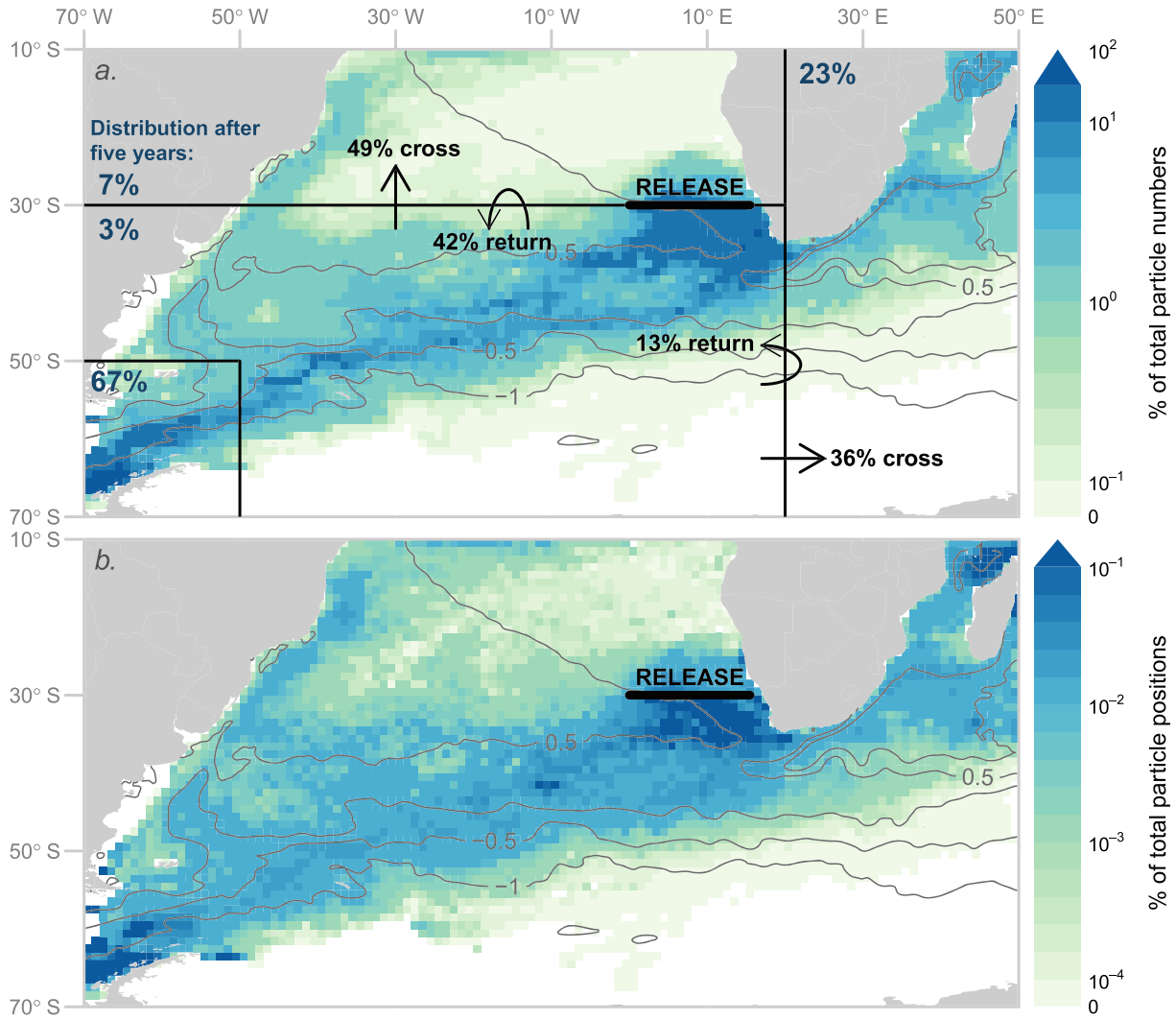

Figure 9. Same as Figure 7 but for Markov chain particles initialized in the BEC along the black line (30°S–29°S; 0°–15°E) and tracked backward for 5 years. (a) Markov chain particle distribution normalized by the total number of released particles. (b) Distribution normalized by the total number of particle positions over the course of 5 years. Refer to the Figure 7 caption for additional details.

Recall that the majority of DP surface drifters that reach the BEC pass through the northern part of the DP (Figure 2). Here we find instead a substantial number of particles passing through the southern section of the DP, as well as the northern section (Figure 9a). The second largest source of the BEC are particles originating east of 20°E in the AR (23%; Figure 9a). Within the AR, particles mostly follow the narrow AC before leaking into the SA (Figures 9a and 9b).

A fraction of particles (10%) cannot be traced back to either the DP or the AR over the 5 years. Most of these (7%) originate north of 30°S. These particles are primarily located in the western limb of the subtropical gyre (Figure 9a), but they also occupy portions of the gyre interior, as evidenced by the high concentrations between 30°S and 10°S (Figure 9b). A smaller portion of these particles (3%) are still located in the southern SA after five (Figure 9a).

Our estimate of the contribution of waters from the DP is substantially higher than most previous studies which range between 6% and 40% (Friocourt et al., 2005; Rodrigues et al., 2010; Rühs et al., 2019; Speich et al., 2001). Our higher estimate likely results from a combination of sampling issues in the vicinity of the AC, which likely does not properly capture the pathway from the AC to the BEC, and the fact that our estimate is derived solely from surface drifters. We note that a direct comparison with previous estimate is

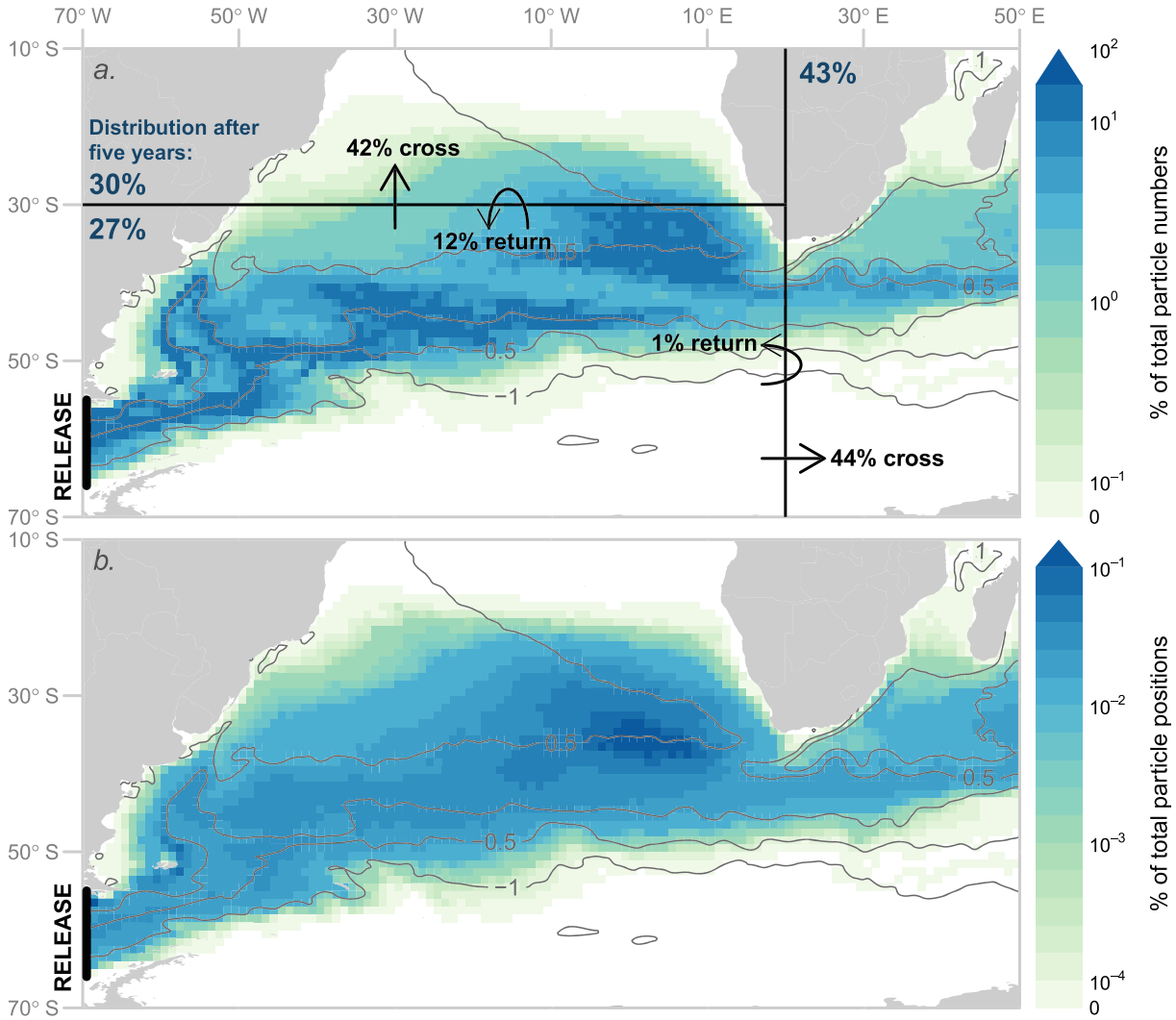

Figure 10. Distribution of Lagrangian particles initialized in the DP along the black line and advected forward for 5 years using the OSCAR fields. (a) Distribution normalized by the total percentage of released particles. (b) Distribution normalized by the total number of particle positions over the course of 5 years. Refer to the caption of Figure 7 for additional details.

challenging due to the use of different methods and different latitudes at which the relative contributions are assessed, ranging from 33°S in Rodrigues et al. (2010) to 20°N in Speich et al. (2001).

As expected, the Markov chain results largely confirm the picture drawn from the drifter record. However, this analysis also reveals additional areas of interaction between the DP and Agulhas waters. Particles released at both sources occupy the Brazil-Malvinas Confluence, the subtropical gyre, and the ARC. From these Markov chain results, we find that the primary source for the BEC are DP waters, with a smaller contribution from the Agulhas and SA. Since the results of the Markov chain are constrained by the availability of drifter data, we next turn to the results of the OSCAR fields as an independent confirmation of our results.

3.3. OSCAR Fields

3.3.1. Drake Passage

As with the Markov chain results, large portions of the SA basin and AR are occupied by particles launched within the DP 5 years previously (Figure 10a). The number of particles following the ACC and the number of particles following the MC upon exiting the DP are approximately the same in these OSCAR results (Figures 10a and 10b), in contrast to the Markov chain results (Figures 7a and 7b). This difference can be partially explained by the poor coverage of the OSCAR fields and drifter trajectories south of 60°S, which gives preference to more northerly pathways such as the MC and the South Atlantic Current.

As also observed in the Markov chain results (Figures 7a and 7b), particles initialized within the DP are densely concentrated in the eastern portion of the subtropical gyre as a result of convergence at the ocean surface (Figures 10a and 10b). Also similar to the previous results (Figures 7a and 7b), OSCAR particles that reach the BEC from the DP are more concentrated toward the western and central parts of the BEC (Figures 10a and 10b).

Most particles released within the DP exit the domain in the well-defined ARC (Figure 10a), with some particles reaching as far north as 10°S in the AR, where they recirculate between the AC and ARC (Figures 10a and 10b). This spread of particles from the DP into the AR again highlights the coexistence of DP and Agulhas waters in a number of areas of the domain. A small percentage of particles (1%) leak back into the South Atlantic after crossing into the AR, similar to the shortcut pathway observed from the drifter record (Figure 5).

After 5 years, the largest amount of particles are located east of 20°E in the AR (43%), with the remaining particles almost equally distributed in the northern (30%) and southern (27%) portions of the subtropical gyre (Figure 10a).

3.3.2. Agulhas Region

Approximately one fifth of the particles released in the AC leak into the SA (Figure 11a). This estimate is very similar to the leakage calculated from the Markov chain (19%; Figure 10a) and, again, lower than estimates from past literature (Durgadoo et al., 2013; McAdam & van Sebille, 2018; Richardson, 2007; van Sebille et al., 2009). The majority of these leaked particles in the OSCAR results are found in the northern SA (15%), with a smaller fraction flowing toward the Brazil-Malvinas Confluence and found in the southern SA (5%; Figure 11a). The high concentrations observed near the western limb of the subtropical gyre (Figure 11b) result from the recirculation of a small number of particles (Figure 11a). The rest of the particles launched in the AC (80%) remain east of 20°E in the AR, or return to the AR after retroflecting in the ARC (Figures 11a and 11b). These particles are most densely concentrated in the narrow AC (Figure 11a) but also show strong recirculations in its vicinity (Figure 11b). These observations are remarkably consistent with the results of the Markov chain (Figures 8a and 8b), derived from a completely independent data set.

We again point out that particles released within the DP (Figures 10a and 10b) and particles released in the AC (Figures 11a and 11b) largely occupy the same regions in the domain. Specifically, they share pathways in the Brazil-Malvinas Confluence, the subtropical gyre, and the ARC, as previously suggested by the Markov chain results (Figures 7a, 7b, 8a, and 8b).

3.3.3. Benguela Current

The results from the OSCAR fields show that over the course of 5 years, the largest source of the BEC are particles originating east of 20°E in the AR (62%; Figure 12a). About half as many particles (33%) can be traced back to the DP, and the remainder are found in the northern (4%) and southern SA (1%; Figure 12a). With the caveat that these estimates are strictly derived from the surface flow, this distribution of source waters is in better agreement than the Markov chain results with a previous observational study by Rodrigues et al. (2010) that attributed a direct contribution from the DP of 4.7Sv (36%) and Agulhas leakage of 8.5Sv (64%). Model results from Rühs et al. (2019) found contributions of 40% and 60% from the DP and Agulhas Leakage, respectively, though their contributions were measured at the North Brazil Current and not the BEC. Keeping in mind the small number of floats in the vicinity of the BEC (15), the results are also in agreement with the distribution of float trajectories (Figure 5b).

However, this distribution differs from the results of the Markov chain (Figures 9a and 9b), which revealed the DP to be a larger contributor (67%) to the source waters of the BEC than the AR (23%). This discrepancy is likely a consequence of insufficient drifter coverage in the vicinity of the BEC. As discussed in the context of the drifter trajectories, very few drifters that arrive in the BEC can be traced back to the AR (Figure 6a). In other words, the drifters may not accurately capture the available pathways. We also note that the difference in this DP and AR divide may be due to an inadequacy on the part of the OSCAR fields. In particular, the OSCAR fields have a limited latitudinal extent and at times do not cover portion of the ACC. Hence, the OSCAR fields might be undersampling the number of particles that are traced back to the DP.

The majority of particles that can be traced back to the DP are concentrated in the northern section of the DP (Figure 12a), a preferential pathway previously observed in the drifter trajectories (Figure 2a). Particles coming from the DP are entrained in the MC and subsequently reach the BEC in the wide South Atlantic Current

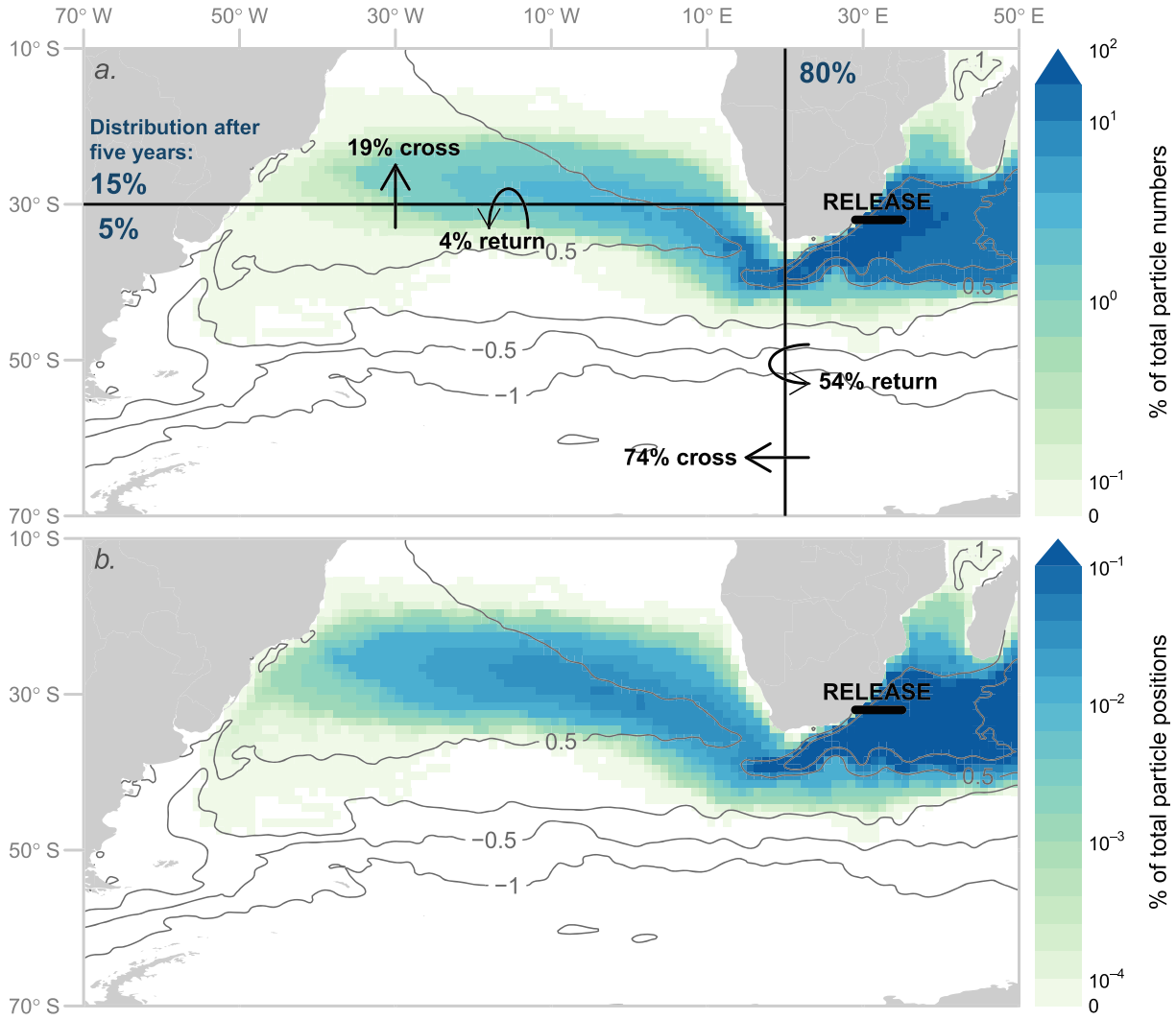

Figure 11. Distribution of Lagrangian particles initialized in the AC along the black line and advected forward for 5 years using the OSCAR fields. (a) Distribution normalized by the total percentage of released particles. (b) Distribution normalized by the total number of particle positions over the course of 5 years. Refer to the caption of Figure 7 for additional details.

(Figure 12a). Note that prior to their arrival in the BEC, a small number of particles originating in the DP flow east of 20°E into the AR, again highlighting a conflation between the DP and AR sources (Figures 12a and 12b).

The particles that can be traced back to the AR mostly flow through the AC and are closely confined to the South African coast (Figure 12a). Similar to the particles from the DP, they exhibit strong recirculations along their pathways, as indicated by the elevated particle concentration in the AR and along the South Atlantic Current (Figure 12b).

In summary, the OSCAR results for particles released in the DP and AC are in good agreement with the results from the drifters, floats, and the Markov chain. Specifically, these OSCAR results yield similar quantitative estimates for the DP and AC distributions and highlight the same areas for interaction between the DP and Agulhas waters. We do note that the particle distributions of the Markov chain are generally more dispersive than those from the OSCAR fields. In other words, the Markov particles (Figures 7–9) occupy a larger portion of the domain after a period of 5 years than the OSCAR particles (Figures 10–12). In part, this difference can be explained by the two methodologies. The Markov chain may be connecting areas of the domain that are not connected in the original drifter data set, as explained earlier in the context of artificial dispersion.

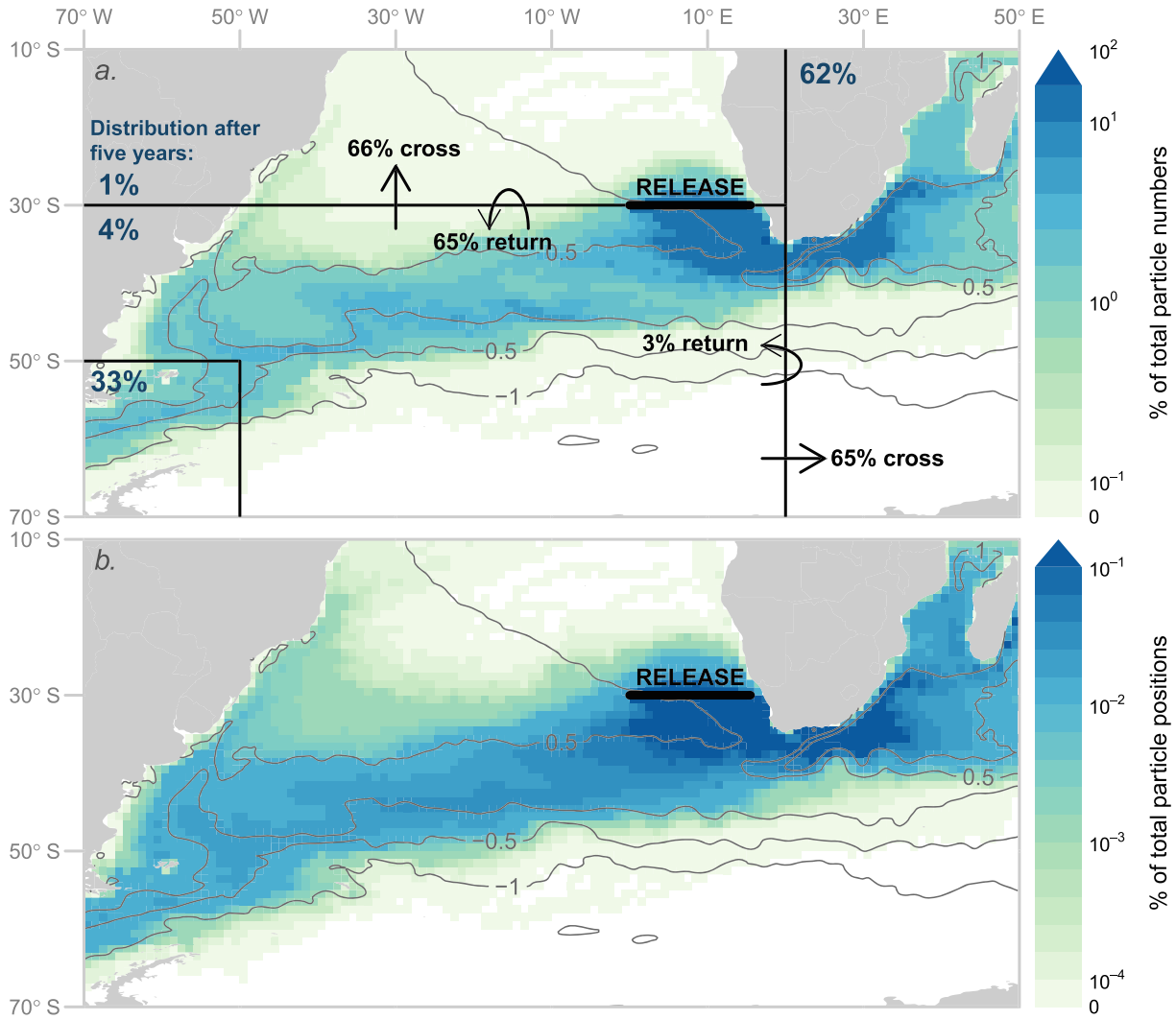

Figure 12. Distribution of Lagrangian particles initialized in the BEC along the black line and advected backward for 5 years using the OSCAR fields. (a) Distribution normalized by the total percentage of released particles. (b) Distribution normalized by the total number of particle positions over the course of 5 years. Refer to the caption of Figure 7 for additional details.

The backward particle advection using the OSCAR fields attributes a larger source contribution to the AR than the DP, while the Markov chain showed a larger contribution for the DP. Many past studies state that the DP contribution is negligible compared to the AR input (Donners & Drijfhout, 2004; Speich et al., 2001; Speich et al., 2007). However, keeping the caveat of two dimensionality in mind, our results indicate that the two contributions are more comparable, as suggested by Rodrigues et al. (2010) and Rühs et al. (2019).

4. Conclusion

This study investigated the surface pathways of the SA and revisited the Indian and Pacific Ocean source waters of the AMOC using observational data. Limitations imposed by the drifter data set were addressed using a Markov chain and Lagrangian particle advections using OSCAR surface fields. Given the remaining surface constraint, areas with known subsurface pathways were excluded from the analysis. We summarize the key findings below.

As in previous studies, DP waters preferentially cross the extended SA basin in the ACC or enter it through the MC, with waters crossing through the northern DP generally following the latter. Over 5 years, DP waters tend to accumulate in the eastern portion of the subtropical gyre.

AR waters mostly recirculate within the AR or exit toward the central Indian Ocean via the Agulhas Return Current. AC waters leaking into the SA tend to be more concentrated on the West African coast than DP waters but also largely recirculate in the subtropical gyre.

Additionally, this study shows that waters entrained in the ACC can escape to join the SAC and vice versa, further east than suggested in previous studies (Boebel et al., 1999; Speich et al., 2001). Our observation is, therefore, in agreement with a recent modeling study by Rühs et al. (2019). Some waters from the DP enter the AR and potentially reenter the SA basin via the leakage route without recirculating in the Indian Ocean subtropical gyre. The Agulhas leakage is at the lower end of previous estimates from the literature, which is particularly the case for the estimate based on the drifter trajectories, as previous estimates had included undrogued drifters (Richardson, 2007; van Sebille et al., 2009). We highlight that the estimate is highly sensitive to the chosen subsetting criteria.

Over the course of 5 years, the primary surface source waters of the BEC are composed of AC waters, DP waters, and local SA waters. While the backward Markov chain and OSCAR results are not in quantitative agreement, both suggest that the DP inflow makes a sizable contribution to the source waters of the BEC region and potentially the upper limb circulation of the AMOC. We highlight the varying traveling times of these source waters, with the DP waters taking approximately twice as long to reach the BEC as the AC waters at the ocean surface.

Multiple surface pathways exist that allow for the interaction between the traditional cold and warm routes. Specifically, the AC region, the BEC region, the eastern portion of the subtropical gyre, and the Brazil-Malvinas Confluence. This interaction suggests that the properties associated with these two source regions may be indistinguishable by the time these waters flow out of the SA subtropical region (see Rühs et al., 2019). Given that both source waters are strongly represented in the gyre interior, we postulate that gyre dynamics also have an impact on setting the properties of the upper limb.

Acknowledgments
The Global Drifter Program data from NOAA is publically available at https://www.aoml.noaa.gov/phod/gdp/index.php website. The Ocean Surface Current Analysis Real-time generated by Earth Space Research is publically available at https://podaac.jpl.nasa.gov/dataset/OSCAR_L4_OC_third-deg website. The subsurface float data from the World Ocean Circulation Experiment Subsurface Float Data Assembly Center at Woods Hole is publically available at https://www.aoml.noaa.gov/phod/float_traj/data2.php website. This work is supported by the Physical Oceanography Program at the National Science Foundation. We are grateful to Sijia Zou and Siren Rühs for their helpful discussions and comments. We thank two anonymous reviewers for carefully considering our manuscript and providing valuable feedback. Finally, we would like to thank Eric Monson from the Data Visualization team at Duke for his expertise and advice regarding our figures.

References

Beal, L. M., De Ruijter, W. P., Biastoch, A., Zahn, R., Cronin, M., Hermes, J., & Baker-Yeboah, S. (2011). On the role of the Agulhas system in ocean circulation and climate. *Nature*, *472*(7344), 429–436. https://doi.org/10.1038/nature09983

Berti, S., Santos, F. A. D., Lacorata, G., & Vulpiani, A. (2011). Lagrangian drifter dispersion in the southwestern Atlantic Ocean. *Journal of Physical Oceanography*, *41*(9), 1659–1672. https://doi.org/10.1175/2011JPO4541.1

Biastoch, A., Böning, C. W., Schwarzkopf, F. U., & Lutjeharms, J. R. (2009). Increase in Agulhas leakage due to poleward shift of Southern Hemisphere westerlies. *Nature*, *462*(7272), 495–498. https://doi.org/10.1038/nature08519

Biastoch, A., & Krauss, W. (1999). The role of mesoscale eddies in the source regions of the Agulhas Current. *Journal of Physical Oceanography*, *29*(9), 2303–2317. https://doi.org/10.1175/1520-0485(1999)029<2303:TROMEI>2.0.CO;2

Boebel, O., Davis, R., Ollitrault, M., Peterson, R., Richardson, P., Schmid, C., & Zenk, W. (1999). The intermediate depth circulation of the western South Atlantic. *Geophysical Research Letters*, *26*(21), 3329–3332. https://doi.org/10.1029/1999GL002355

Boebel, O., Lutjeharms, J., Schmid, C., Zenk, W., Rossby, T., & Barron, C. (2003). The Cape Cauldron: A regime of turbulent inter-ocean exchange. *Deep Sea Research Part II: Topical Studies in Oceanography*, *50*(1), 57–86. https://doi.org/10.1016/S0967-0645(02)00379-X

Bonjean, F., & Lagerloef, G. S. (2002). Diagnostic model and analysis of the surface currents in the tropical Pacific Ocean. *Journal of Physical Oceanography*, *32*(10), 2938–2954. https://doi.org/10.1175/1520-0485(2002)032<2938:DMAAOT>2.0.CO;2

De Ruijter, W. (1982). Asymptotic analysis of the Agulhas and Brazil Current systems. *Journal of Physical Oceanography*, *12*(4), 361–373. https://doi.org/10.1175/1520-0485(1982)012<0361:AAOTAA>2.0.CO;2

Dohan, K., & Maximenko, N. (2010). Monitoring ocean currents with satellite sensors. *Oceanography*, *23*(4), 94–103. https://doi.org/10.5670/oceanog.2010.08

Donners, J., & Drijfhout, S. (2004). The Lagrangian view of South Atlantic interocean exchange in a global ocean model compared with inverse model results. *Journal of Physical Oceanography*, *34*(5), 1019–1035. https://doi.org/10.1175/1520-0485(2004)034<1019:TLVOSA>2.0.CO;2

Durgadoo, J. V., Loveday, B. R., Reason, C. J., Penven, P., & Biastoch, A. (2013). Agulhas leakage predominantly responds to the Southern Hemisphere westerlies. *Journal of Physical Oceanography*, *43*(10), 2113–2131. https://doi.org/10.1175/JPO-D-13-047.1

Friocourt, Y., Drijfhout, S., Blanke, B., & Speich, S. (2005). Water mass export from Drake Passage to the Atlantic, Indian, and Pacific oceans: A Lagrangian model analysis. *Journal of Physical Oceanography*, *35*(7), 1206–1222. https://doi.org/10.1175/JPO2748.1

Garzoli, S. L. (1993). Geostrophic velocity and transport variability in the Brazil-Malvinas Confluence. *Deep Sea Research Part I: Oceanographic Research Papers*, *40*(7), 1379–1403. https://doi.org/10.1016/0967-0637(93)90118-M

Garzoli, S. L., & Gordon, A. L. (1996). Origins and variability of the Benguela Current. *Journal of Geophysical Research*, *101*(C1), 897–906. https://doi.org/10.1029/95JC03221

Garzoli, S. L., & Matano, R. (2011). The South Atlantic and the Atlantic meridional overturning circulation. *Deep Sea Research Part II: Topical Studies in Oceanography*, *58*(17-18), 1837–1847. https://doi.org/10.1016/j.dsr2.2010.10.063

Gordon, A. L. (1986). Interocean exchange of thermocline water. *Journal of Geophysical Research*, *91*(C4), 5037–5046. https://doi.org/10.1029/JC091iC04p05037

Gordon, A. L., Weiss, R. F., Smethie, W. M. Jr., & Warner, M. J. (1992). Thermocline and intermediate water communication between the South Atlantic and Indian Oceans. *Journal of Geophysical Research*, *97*(C5), 7223–7240. https://doi.org/10.1029/92JC00485

Johns, W. E., Lee, T., Beardsley, R., Candela, J., Limeburner, R., & Castro, B. (1998). Annual cycle and variability of the North Brazil Current. *Journal of Physical Oceanography*, *28*(1), 103–128. https://doi.org/10.1175/1520-0485(1998)028<0103:ACAVOT>2.0.CO;2

Johnson, E. S., Bonjean, F., Lagerloef, G. S., Gunn, J. T., & Mitchum, G. T. (2007). Validation and error analysis of OSCAR sea surface currents. *Journal of Atmospheric and Oceanic Technology*, *24*(4), 688–701. https://doi.org/10.1175/JTECH1971.1

Jullion, L., Heywood, K. J., Naveira Garabato, A. C., & Stevens, D. P. (2010). Circulation and water mass modification in the Brazil-Malvinas Confluence. *Journal of Physical Oceanography*, *40*(5), 845–864. https://doi.org/10.1175/2009JPO4174.1

Killworth, P. D., & Hughes, C. W. (2002). The Antarctic Circumpolar Current as a free equivalent-barotropic jet. *Journal of Marine Research*, *60*(1), 19–45. https://doi.org/10.1357/002224002762341230

LaCasce, J. H. (2008). Statistics from Lagrangian observations. *Progress in Oceanography*, *77*(1), 1–29. https://doi.org/10.1016/j.pocean.2008.02.002

Laurindo, L. C., Mariano, A. J., & Lumpkin, R. (2017). An improved near-surface velocity climatology for the global ocean from drifter observations. *Deep Sea Research Part I: Oceanographic Research Papers*, *124*, 73–92. https://doi.org/10.1016/j.dsr.2017.04.009

Lee, S. K., Lumpkin, R., Baringer, M. O., Meinen, C. S., Goes, M., Dong, S., et al. (2019). Global meridional overturning circulation inferred from a data-constrained ocean and sea-ice model. *Geophysical Research Letters*, *46*, 1521–1530. https://doi.org/10.1029/2018GL080940

Lumpkin, R., Grodsky, S. A., Centurioni, L., Rio, M.-H., Carton, J. A., & Lee, D. (2013). Removing spurious low-frequency variability in drifter velocities. *Journal of Atmospheric and Oceanic Technology*, *30*(2), 353–360. https://doi.org/10.1175/JTECH-D-12-00139.1

Lumpkin, R., & Pazos, M. (2007). Measuring surface currents with Surface Velocity Program drifters: The instrument, its data, and some recent results. In A. Griffa, A. de Kirwan, Jr., A. Mariano, T. Özgökmen, & T. Rossby (Eds.), *Lagrangian analysis and prediction of coastal and ocean dynamics* (pp. 39–67). Cambridge: Cambridge University Press.

Macdonald, A. M. (1998). The global ocean circulation: A hydrographic estimate and regional analysis. *Progress in Oceanography*, *41*(3), 281–382. https://doi.org/10.1016/S0079-6611(98)00020-2

Mariano, A. J., Griffa, A., Özgökmen, T. M., & Zambianchi, E. (2002). Lagrangian analysis and predictability of coastal and ocean dynamics 2000. *Journal of Atmospheric and Oceanic Technology*, *19*(7), 1114–1126. https://doi.org/10.1175/1520-0426(2002)019<1114:LAAPOC>2.0.CO;2

Mason, E., Pascual, A., Gaube, P., Ruiz, S., Pelegrí, J. L., & Delepoulle, A. (2017). Subregional characterization of mesoscale eddies across the Brazil-Malvinas Confluence. *Journal of Geophysical Research: Oceans*, *122*, 3329–3357. https://doi.org/10.1002/2016JC012611

McAdam, R., & van Sebille, E. (2018). Surface connectivity and interocean exchanges from drifter-based transition matrices. *Journal of Geophysical Research: Oceans*, *123*, 514–532. https://doi.org/10.1002/2017JC013363

Miron, P., Beron-Vera, F. J., Olascoaga, M. J., Froyland, G., Pérez-Brunius, P., & Sheinbaum, J. (2019). Lagrangian geography of the deep Gulf of Mexico. *Journal of Physical Oceanography*, *49*(1), 269–290. https://doi.org/10.1175/JPO-D-18-0073.1

Miron, P., Beron-Vera, F. J., Olascoaga, M. J., Sheinbaum, J., Pérez-Brunius, P., & Froyland, G. (2017). Lagrangian dynamical geography of the Gulf of Mexico. *Scientific Reports*, *7*(1), 7021. https://doi.org/10.1038/s41598-017-07177-w

Niiler, P. P., & Paduan, J. D. (1995). Wind-driven motions in the northeast Pacific as measured by Lagrangian drifters. *Journal of Physical Oceanography*, *25*(11), 2819–2830. https://doi.org/10.1175/1520-0485(1995)025<2819:WDMITN>2.0.CO;2

Olson, D. B., Podesta, G. P., Evans, R. H., & Brown, O. B. (1988). Temporal variations in the separation of Brazil and Malvinas Currents. *Deep Sea Research Part A. Oceanographic Research Papers*, *35*(12), 1971–1990. https://doi.org/10.1016/0198-0149(88)90120-3

Pazan, S. E., & Niiler, P. P. (2001). Recovery of near-surface velocity from undrogued drifters. *Journal of Atmospheric and Oceanic Technology*, *18*(3), 476–489. https://doi.org/10.1175/1520-0426(2001)018<0476:RONSVF>2.0.CO;2

Peterson, R. G., & Stramma, L. (1991). Upper-level circulation in the South Atlantic Ocean. *Progress in Oceanography*, *26*(1), 1–73. https://doi.org/10.1016/0079-6611(91)90006-8

Richardson, P. L. (2007). Agulhas leakage into the Atlantic estimated with subsurface floats and surface drifters. *Deep Sea Research Part I: Oceanographic Research Papers*, *54*(8), 1361–1389. https://doi.org/10.1016/j.dsr.2007.04.010

Rintoul, S. R. (1991). South Atlantic interbasin exchange. *Journal of Geophysical Research*, *96*(C2), 2675–2692. https://doi.org/10.1029/90JC02422

Rodrigues, R. R., Wimbush, M., Watts, D. R., Rothstein, L. M., & Ollitrault, M. (2010). South Atlantic mass transports obtained from subsurface float and hydrographic data. *Journal of Marine Research*, *68*(6), 819–850. https://doi.org/10.1357/002224010796673858

Rühs, S., Durgadoo, J. V., Behrens, E., & Biastoch, A. (2013). Advective timescales and pathways of Agulhas leakage. *Geophysical Research Letters*, *40*, 3997–4000. https://doi.org/10.1002/grl.50782

Rühs, S., Schwarzkopf, F. U., Speich, S., & Biastoch, A. (2019). Cold vs. warm water route—Sources for the upper limb of the Atlantic Meridional Overturning Circulation revisited in a high-resolution ocean model. *Ocean Science*, *15*(3), 489–512. https://doi.org/10.5194/os-15-489-2019

Schmid, C. (2014). Mean vertical and horizontal structure of the subtropical circulation in the South Atlantic from three-dimensional observed velocity fields. *Deep Sea Research Part I: Oceanographic Research Papers*, *91*, 50–71. https://doi.org/10.1016/j.dsr.2014.04.015

Schott, F. A., Dengler, M., Zantopp, R., Stramma, L., Fischer, J., & Brandt, P. (2005). The shallow and deep western boundary circulation of the South Atlantic at 5–11 S. *Journal of Physical Oceanography*, *35*(11), 2031–2053. https://doi.org/10.1175/JPO2813.1

Schott, F. A., Fischer, J., & Stramma, L. (1998). Transports and pathways of the upper-layer circulation in the western tropical Atlantic. *Journal of Physical Oceanography*, *28*(10), 1904–1928. https://doi.org/10.1175/1520-0485(1998)028<1904:TAPOTU>2.0.CO;2

Sloyan, B. M., & Rintoul, S. R. (2001). The Southern Ocean limb of the global deep overturning circulation. *Journal of Physical Oceanography*, *31*(1), 143–173. https://doi.org/10.1175/1520-0485(2001)031<0143:TSOLOT>2.0.CO;2

Speich, S., Blanke, B., & Cai, W. (2007). Atlantic meridional overturning circulation and the Southern Hemisphere supergyre. *Geophysical Research Letters*, *34*, L23614. https://doi.org/10.1029/2007GL031583

Speich, S., Blanke, B., & Madec, G. (2001). Warm and cold water routes of an O.G.C.M. thermohaline conveyor belt. *Geophysical Research Letters*, *28*(2), 311–314. https://doi.org/10.1029/2000gl011748

Stramma, L. (1991). Geostrophic transport of the South Equatorial Current in the Atlantic. *Journal of Marine Research*, *49*(2), 281–294. https://doi.org/10.1357/002224091784995864

Stramma, L., & England, M. (1999). On the water masses and mean circulation of the South Atlantic Ocean. *Journal of Geophysical Research*, *104*(C9), 20,863–20,883. https://doi.org/10.1029/1999JC900139

van der Mheen, M., Pattiaratchi, C., & van Sebille, E. (2019). Role of Indian ocean dynamics on accumulation of buoyant debris. *Journal of Geophysical Research: Oceans*, *124*, 2571–2590. https://doi.org/10.1029/2018JC014806

van Sebille, E., Beal, L. M., & Johns, W. E. (2011). Advective time scales of Agulhas leakage to the North Atlantic in surface drifter observations and the 3D OFES model. *Journal of Physical Oceanography*, *41*(5), 1026–1034. https://doi.org/10.1175/2010JPO4602.1

van Sebille, E., England, M. H., & Froyland, G. (2012). Origin, dynamics and evolution of ocean garbage patches from observed surface drifters. *Environmental Research Letters*, *7*(4). https://doi.org/10.1088/1748-9326/7/4/044040

van Sebille, E., Griffies, S. M., Abernathey, R., Adams, T. P., Berloff, P., Biastoch, A., & Cotter, C. J. (2018). Lagrangian ocean analysis: Fundamentals and practices. *Ocean Modelling*, *121*, 49–75. https://doi.org/10.1016/j.ocemod.2017.11.008

van Sebille, E., van Leeuwen, P. J., Biastoch, A., Barron, C. N., & De Ruijter, W. P. M. (2009). Lagrangian validation of numerical drifter trajectories using drifting buoys: Application to the Agulhas system. *Ocean Modelling*, *29*(4), 269–276. https://doi.org/10.1016/j.ocemod.2009.05.005

Weijer, W., De Ruijter, W. P., Sterl, A., & Drijfhout, S. S. (2002). Response of the Atlantic overturning circulation to South Atlantic sources of buoyancy. *Global and Planetary Change*, *34*(3-4), 293–311. https://doi.org/10.1016/S0921-8181(02)00121-2

Weijer, W., & van Sebille, E. (2014). Impact of Agulhas Leakage on the Atlantic Overturning Circulation in the CCSM4. *Journal of Climate*, *27*(1), 101–110. https://doi.org/10.1175/jcli-d-12-00714.1

Willson, H. R., & Rees, N. (2000). Classification of mesoscale features in the Brazil-Falkland Current Confluence zone. *Progress in Oceanography*, *45*(3-4), 415–426. https://doi.org/10.1016/S0079-6611(00)00011-2

You, Y. (2002). Quantitative estimate of Antarctic Intermediate Water contributions from the Drake Passage and the southwest Indian Ocean to the South Atlantic. *Journal of Geophysical Research*, *107*(C4), 3031. https://doi.org/10.1029/2001JC000880